Check for updates

AGU ADVANCING EARTH AND SPACE SCIENCES

Water Resources Research

RESEARCH ARTICLE
10.1029/2025WR040033

Key Points:

- Typhoons and extreme drought caused severe saltwater intrusion in the Changjiang Estuary in 2022, critically threatening the water supply
- The Three Gorges Reservoir released 4.063×10^9 m^3 of freshwater to mitigate saltwater intrusion and ensure the area's freshwater supply
- Strong northerly winds during the cold front reduced the release's effectiveness, shortening the Qingcaosha Reservoir's water intake period

Correspondence to:
W. Qiu,
qiuwei@mail.crsri.cn

Citation:
Qiu, W., Zhu, J., Luan, H., Wu, T., Li, L., Qu, G., et al. (2025). Saltwater intrusion and emergency freshwater release in the Changjiang River estuary under extreme drought conditions. *Water Resources Research*, *61*, e2025WR040033. https://doi.org/10.1029/2025WR040033

Received 29 JAN 2025
Accepted 6 AUG 2025

Author Contributions:
Conceptualization: Wei Qiu
Data curation: Wei Qiu, Rui Ma
Formal analysis: Wei Qiu
Funding acquisition: Wei Qiu, Jianrong Zhu, Hualong Luan, Geng Qu
Investigation: Wei Qiu, Rui Ma
Methodology: Wei Qiu, Jianrong Zhu, Linjiang Li, Carlo Gualtieri
Project administration: Wei Qiu
Resources: Wei Qiu
Software: Wei Qiu, Jianrong Zhu
Supervision: Wei Qiu
Validation: Wei Qiu, Tong Wu, Rui Ma
Visualization: Wei Qiu, Tong Wu
Writing – original draft: Wei Qiu
Writing – review & editing: Wei Qiu, Hualong Luan, Linjiang Li, Geng Qu, Carlo Gualtieri

© 2025. The Author(s).
This is an open access article under the terms of the Creative Commons Attribution-NonCommercial-NoDerivs License, which permits use and distribution in any medium, provided the original work is properly cited, the use is non-commercial and no modifications or adaptations are made.

Saltwater Intrusion and Emergency Freshwater Release in the Changjiang River Estuary Under Extreme Drought Conditions

Wei Qiu[1,2], Jianrong Zhu[3,4], Hualong Luan[1,2], Tong Wu[5], Linjiang Li[6], Geng Qu[1,2], Rui Ma[3], and Carlo Gualtieri[7]

[1]River Research Department, Changjiang River Scientific Research Institute, Wuhan, P. R. China, [2]Key Laboratory of River and Lake Regulation and Flood Control in the Middle and Lower Reaches of the Changjiang River of Ministry of Water Resources, Wuhan, P. R. China, [3]State Key Laboratory of Estuarine and Coastal Research, East China Normal University, Shanghai, P. R. China, [4]Shanghai Engineering Research Center of Water Environment Simulation and Ecological Restoration, Shanghai, P. R. China, [5]Yangtze River Navigation Survey and Design Institute (Wuhan) Co., Ltd, Wuhan, P. R. China, [6]Shanghai Typhoon Institute, China Meteorological Administration, Shanghai, P. R. China, [7]Department of Structures for Engineering and Architecture (DIST), University of Napoli Federico II, Napoli, Italy

Abstract Releasing freshwater from upstream reservoirs is a reasonable strategy to mitigate saltwater intrusion, however, its effectiveness may vary depending on weather events. Previous studies have primarily examined the effects on saltwater intrusion of seasonal regulation in reservoir discharge, with a limited attention given to the synoptic scale. This study applied the ECOM-si to quantitatively analyze the impacts of the October 2022 emergency freshwater release on saltwater intrusion, also elucidating the mechanisms by which cold fronts (defined as northerly winds with speeds exceeding 10 m/s) impaired the effects of that release. The release reduced landward advective salt flux, shifting the 0.45 psu isohaline 17 km downstream during the neap tide period. On October 21, the salinity at the Qingcaosha Reservoir (QCSR) intake point fell to 0.45 psu, creating a 12.75-hr window for freshwater intake. Cold fronts greatly diminished the effectiveness of freshwater release, shortening the water intake period by 24.14 hr. During the cold front period, northerly winds induced landward Ekman transport, creating a horizontal recirculation pattern with inflow through the North Channel (NC) and outflow through the South Channel (SC). The net landward water flux per unit width in the NC reached -1 m^2/s. During the first cold front, steady shear salt flux contributed most significantly, with a magnitude of -70 ton/s, while advective salt flux dominated during the second cold front, reaching -239 ton/s. Without the cold fronts, the potential water intake time could have increased to 36.89 hr.

Plain Language Summary In 2022, the Changjiang River Estuary experienced one of its most severe saltwater intrusion events in nearly five decades due to an extreme drought and the combined impact of typhoons. This phenomenon posed a significant threat to freshwater supplies for Shanghai and surrounding areas. To mitigate this, the Three Gorges Reservoir released 4.063×10^9 m^3 of freshwater downstream. While this release temporarily reduced salinity and allowed for limited water intake, strong northerly winds during cold fronts diminished its overall effectiveness. The study used advanced hydrodynamic modeling to analyze these challenges and found that wind-driven processes, such as landward salt flux, played a critical role in counteracting the freshwater release. Without the influence of cold fronts, the water intake period could have been tripled. These findings offer valuable insights for climate-resilient water management strategies in estuaries facing increasing risks from extreme drought and meteorological disturbances, including systems like the Mekong River estuary.

1. Introduction

Freshwater supply in estuarine regions is essential for sustaining densely populated urban areas and supporting industrial, agricultural, and ecological needs. These regions face increasing threats from saltwater intrusion, exacerbated by climate change, extreme weather events, and human interventions. Saltwater intrusion-the process by which saline water encroaches into freshwater zones-can disrupt water supply, harm ecosystems, and compromise agricultural productivity (Chau et al., 2021; Luo et al., 2024; Zhu et al., 2013). Globally, estuaries are under mounting pressure as rising sea levels, reduced river discharge, intensified storm events, and extreme

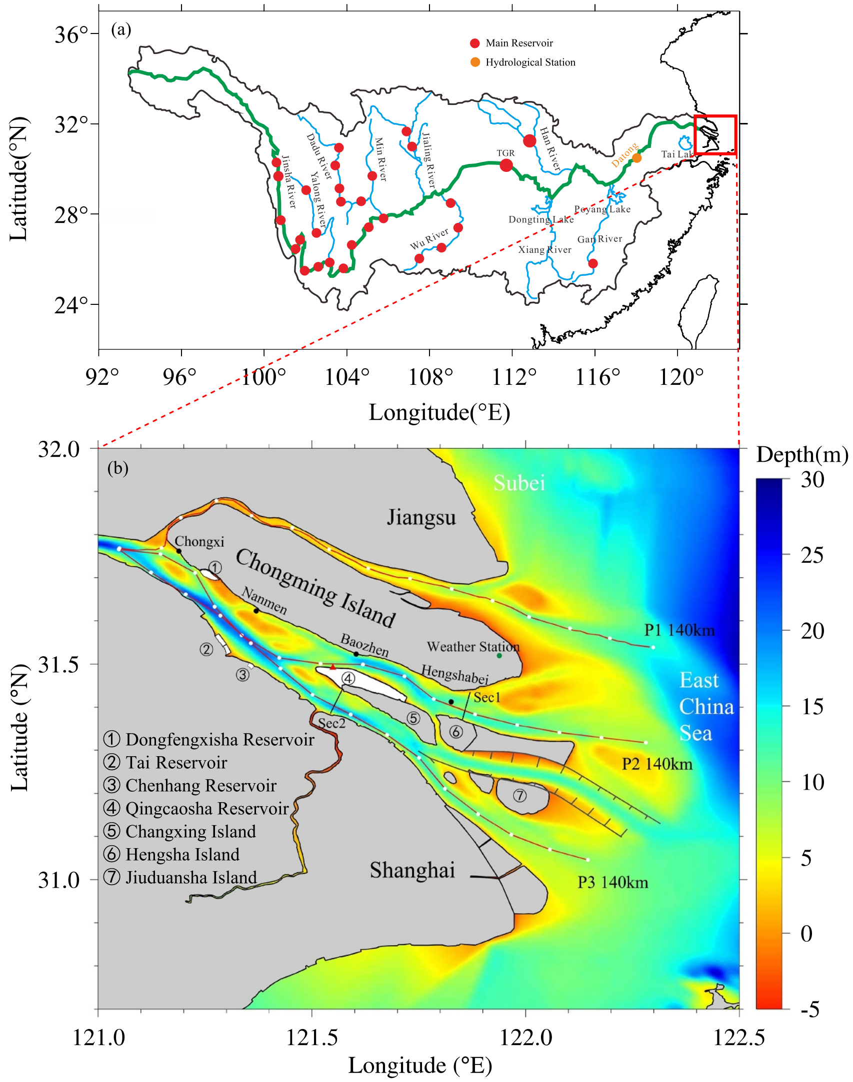

Figure 1. Overview map of the Changjiang River Basin (a) and topographic map of the Changjiang River Estuary (b).

climatic phenomena like droughts and cold fronts amplify the risks of saltwater intrusion (Bellafiore et al., 2021; He et al., 2018; Li et al., 2022; Zhu et al., 2020).

The Changjiang River Estuary, the largest river system in Asia (Figure 1a), is a typical multi-channel estuary with four mouths to the sea (Figure 1b). The long-term (1950–2022) average river discharge at the Datong Hydrological Station is 28,351 m^3/s, with runoff primarily concentrated in the flood season (May–October), exhibiting significant seasonal and interannual variations. This abundant river discharge provides substantial freshwater resources to the estuary region, supporting vital ecological and economic activities. To harness these resources, four estuary reservoirs have been constructed in the South Branch (SB), with the Qingcaosha Reservoir (QCSR) being the largest and most significant. QCSR supplies 70% of Shanghai's freshwater needs, delivering 7.19×10^6 m^3 daily, making it an indispensable water source for the region's population and industries (Chen et al., 2019). However, QCSR faces significant challenges from saltwater intrusion. When salinity levels exceed 0.45 practical salinity units (psu), water intake operations must be suspended, threatening the reliability of freshwater supply. Ensuring the safety and sustainability of this critical resource is therefore essential, particularly during extreme climatic events.

In 2022, the Changjiang River basin experienced its most severe drought since 1961, drastically reducing river discharge during the flood season. The mean river discharge at the Datong hydrological station in September was

19447973, 2025, 8, Downloaded from https://agupubs.onlinelibrary.wiley.com/doi/10.1029/2025WR040033 by Carlo Gualtieri - Uni Federico Ii Di Napoli , Wiley Online Library on [18/08/2025]. See the Terms and Conditions (https://onlinelibrary.wiley.com/terms-and-conditions) on Wiley Online Library for rules of use; OA articles are governed by the applicable Creative Commons License

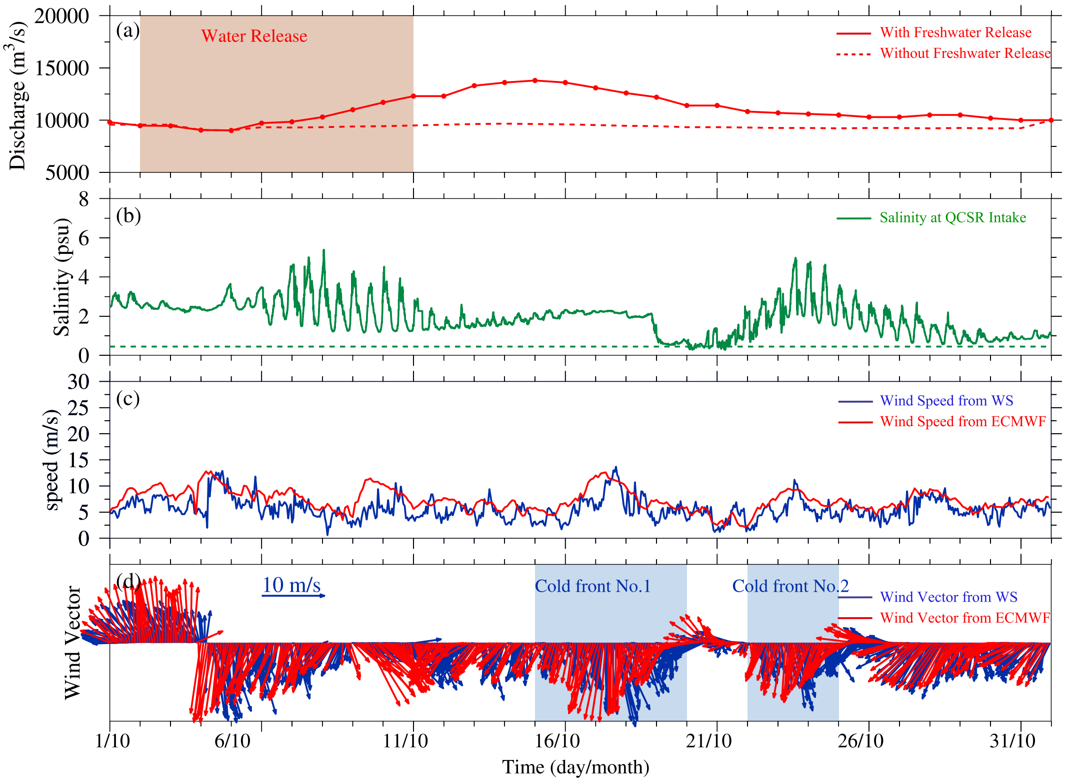

Figure 2. Daily distribution of the measured river discharge at the Datong hydrological station (a), measured salinity at the water intake of the QCSR (b), wind speed (c) and wind vector (d) at Weather Station (WS, Figure 1) in October 2022. (c), (d) blue lines represent the observed data from the Weather Station, while red lines represent the reanalysis data from the European Centre for Medium-Range Weather Forecasts (ECMWF, https://cds.climate.copernicus.eu/cdsapp#!/home).

only 11,861 m^3/s, significantly below the long-term monthly average of 38,873 m^3/s (1950–2022). Combined with the effects of typhoons Hinnamnor, Muifa, and Nanmadol, this severe drought triggered unprecedented saltwater intrusion in the estuary. During this period, the QCSR was unable to intake freshwater for nearly 24 consecutive days, creating a critical freshwater supply challenge for Shanghai and surrounding areas. To mitigate the impact of saltwater intrusion and ensure freshwater availability, the Changjiang River Water Resources Commission implemented emergency freshwater release measures. Between 2 October and 11 October 2022, cascade reservoirs upstream, including the Three Gorges Reservoir (TGR), released over 4.063×10^9 m^3 of freshwater into the downstream estuary (Figure 2a). This emergency release aimed to push seaward the saltwater intrusion, to establish lower salinity levels at the reservoir intake, and restore freshwater supply. Despite these efforts, the observed reduction in salinity at the QCSR was significantly lower than expected, providing only a 12.75-hr intake window (Figure 2b). This outcome raised concerns about the factors limiting the effectiveness of emergency freshwater release.

Cold fronts, marked by strong northerly winds, likely played a critical role in reducing the effectiveness of the freshwater release (Li et al., 2012; H. Wu et al., 2010; Xue et al., 2009; Zhang et al., 2019; Zhu et al., 2020). During the water supply period, two cold fronts occurred (Figures 2c and 2d), altering the balance between landward and seaward transport processes through mechanisms such as wind-driven Ekman transport and changes in estuarine circulation (Aristizábal & Chant, 2015; Duran et al., 2016; Geyer, 1997; Giddings & MacCready, 2017; Li et al., 2020). These cold fronts likely counteracted the effects of the emergency freshwater release, reducing its ability to repel saltwater and lower salinity effectively. This interplay between freshwater release and meteorological events highlights the complexity of managing freshwater resources in dynamic estuarine systems. Existing research on saltwater intrusion and freshwater management in estuaries has primarily focused on seasonal scales, examining the impact of reservoir regulation during dry seasons or prolonged droughts. Some studies have addressed reservoirs typically releasing freshwater during dry periods to increase downstream discharge, thereby to mitigate saltwater intrusion (Hoang et al., 2019; Qiu & Zhu, 2013; Van

19447973, 2025, 8, Downloaded from https://agupubs.onlinelibrary.wiley.com/doi/10.1029/2025WR040033 by Carlo Gualtieri - Uni Federico Ii Di Napoli , Wiley Online Library on [18/08/2025]. See the Terms and Conditions (https://onlinelibrary.wiley.com/terms-and-conditions) on Wiley Online Library for rules of use; OA articles are governed by the applicable Creative Commons License

19447973, 2025, 8, Downloaded from https://agupubs.onlinelibrary.wiley.com/doi/10.1029/2025WR040033 by Carlo Gualtieri - Uni Federico Ii Di Napoli , Wiley Online Library on [18/08/2025]. See the Terms and Conditions (https://onlinelibrary.wiley.com/terms-and-conditions) on Wiley Online Library for rules of use; OA articles are governed by the applicable Creative Commons License

et al., 2020). However, these studies predominantly focus on long-term discharge variations, and only few have examined how synoptic-scale atmospheric events, such as cold fronts, interact with short-term emergency freshwater releases. The mechanisms through which cold fronts influence the effectiveness of freshwater release also remain poorly understood. This study addresses that gap by quantitatively analyzing the short-term response of estuarine salinity dynamics to emergency freshwater releases under the influence of cold fronts, thereby providing new insights into saltwater intrusion management at the synoptic scale.

This study aims to address these knowledge gaps by quantitatively analyzing the effects of emergency freshwater release during the extreme saltwater intrusion event of 2022. Specifically, it seeks to: (a) quantify the impact of emergency freshwater release on salinity reduction in the Changjiang River Estuary during the severe drought of 2022, (b) analyze the influence of cold fronts on the effectiveness of these operations, and (c) elucidate the mechanisms by which cold fronts affected estuarine hydrodynamics and salinity distribution. These findings are aimed at proposing strategies for improving freshwater resource management in estuarine systems under increasingly dynamic environmental conditions.

2. Methods

2.1. Model Setup

In this study, the semi-implicit Estuarine, Coastal, and Ocean Model (ECOM-si) (Blumberg, 1994) was applied. This model was chosen due to its proven capability in simulating three-dimensional hydrodynamics and salinity transport in estuarine systems. H. Wu and Zhu (2010) enhanced ECOM-si by improving the advection scheme, which significantly increased the accuracy of salinity simulations in the Changjiang River Estuary. Additionally, Lyu and Zhu (2018) refined the bottom friction coefficient calculations, which notably improved the accuracy of simulating saltwater spillover (SSO) from the North Branch (NB). These methodological advancements have been critical for accurately reproducing estuarine circulation and saltwater intrusion processes. ECOM-si has since been widely applied in the Changjiang Estuary (Qiu & Zhu, 2015; T. Wu et al., 2023). The simulation domain encompasses the Changjiang River estuary and its adjacent sea regions (Figure 3). The western boundary extends to the Datong hydrological station, which serves as the tidal limit during the dry season. The average daily river discharge recorded at the Datong station was incorporated as the river boundary condition.

The open sea boundaries were driven by total water levels, consisting of residual water level and tidal level, as described by the following equation:

$$\zeta = \overline{\zeta} + \sum_{i}^{15} a_i \cos(\omega_i + g_i) \tag{1}$$

Here, ζ denotes the total water level, $\overline{\zeta}$ represents the residual (mean) water level reflecting the shelf current, and the summation term represents the tidal level. The tidal level is calculated using the harmonic constants of 15 principal tidal constituents (M_2, S_2, N_2, K_2, K_1, O_1, P_1, Q_1, MF, MM, MN_4, M_4, MS_4, S_1, and $2N_2$), where a_i and g_i are the amplitude and phase of each constituent, respectively, derived from the TPXO9 database (https://www.tpxo.net/global/tpxo9-atlas).

Previous studies have demonstrated that wind stress impacts on estuarine hydrodynamics and salinity transport are not purely local; remote winds can generate coastally trapped waves via the Ekman effect, propagating hundreds of kilometers to influence estuarine residual water levels, currents, and salinity (Casares-Salazar & Mariño-Tapia, 2016; Huang & Li, 2017). Such phenomenon was noted during our simulations of the cold front scenario. Due to the relatively small spatial extent of its domain, the small-scale model cannot accurately resolve the effects of remote wind forcing. To improve salinity simulation accuracy under cold front conditions, a model with a large-scale domain encompassing the Bohai Sea, Yellow Sea, and East China Sea was applied to generate open boundary conditions for the small-scale model. This model was driven by ocean circulation, tidal forces, river discharge, and surface winds (H. Wu et al., 2011). Specifically, the large-scale model outputs water level time series that were filtered using a 36-hr low-pass filter to remove tidal signals and isolate residual water levels. These residual water levels were then interpolated to the open boundaries of the small-scale model and used to drive the simulation. It is important to note that the small-scale model was not nested into the large-scale model; instead, boundary conditions were transferred offline.

19447973, 2025, 8, Downloaded from https://agupubs.onlinelibrary.wiley.com/doi/10.1029/2025WR040033 by Carlo Gualtieri - Uni Federico Ii Di Napoli , Wiley Online Library on [18/08/2025]. See the Terms and Conditions (https://onlinelibrary.wiley.com/terms-and-conditions) on Wiley Online Library for rules of use; OA articles are governed by the applicable Creative Commons License

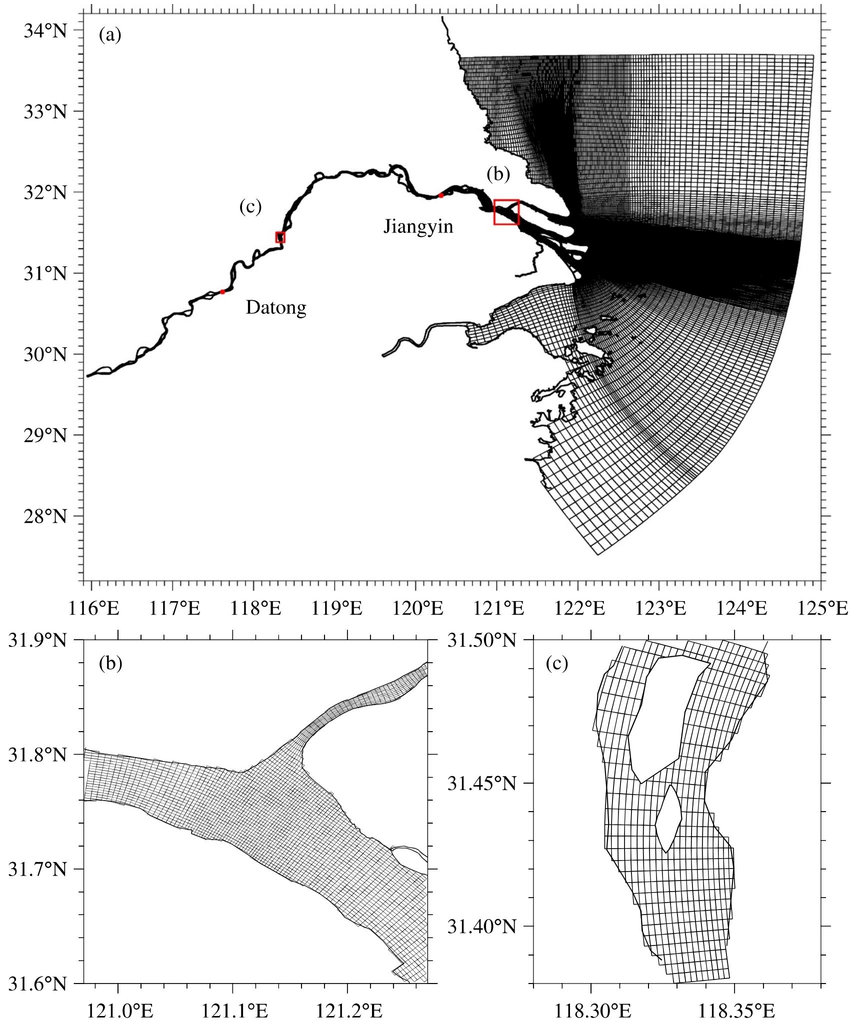

Figure 3. Model domain and grids (a); enlarged view of the model grids around the bifurcation between the NB and SB (b); enlarged view of the model grids at the upper reaches of the river (c).

Wind stress on the sea surface was incorporated, using wind field data from the ECMWF. These data featured a temporal resolution of 1 hr and a spatial resolution of $0.25° \times 0.25°$. The model simulation period spanned from 1 July to 31 October 2022, with a time step of 60 s.

2.2. Model Validation

The ECOM-si model has undergone extensive calibration, validation, and application in numerous prior studies of the Changjiang River estuary, consistently demonstrating its capability to accurately reproduce observed water levels, currents, and salinity (Li et al., 2022; T. Wu et al., 2023). In the present study, salinity data collected from the Chongxi, Nanmen, Baozhen, and Hengshabei hydrological stations during the period of 1–31 October 2022 were utilized to validate the model (see Figure 1 for the locations of hydrological stations; data source: https://doi.org/10.6084/m9.figshare.28245719). The simulation results were assessed using correlation coefficient (CC), skill score (SS), and root mean square error (RMSE) as evaluation metrics, with the respective formulas provided in Appendix A.

Observed salinity at the four stations exhibited a semi-diurnal cycle characterized by two peaks and two troughs per day (Figure 4). At the Chongxi station, salinity maxima occurred during spring tides, while minima coincided with neap tides, primarily influenced by saltwater spillover (SSO) from the NB (Figure 4a). In contrast, salinity at the Baozhen and Hengshabei stations was governed by the direct saltwater intrusion from NC, with maxima

19447973, 2025, 8, Downloaded from https://agupubs.onlinelibrary.wiley.com/doi/10.1029/2025WR040033 by Carlo Gualtieri - Uni Federico Ii Di Napoli , Wiley Online Library on [18/08/2025]. See the Terms and Conditions (https://onlinelibrary.wiley.com/terms-and-conditions) on Wiley Online Library for rules of use; OA articles are governed by the applicable Creative Commons License

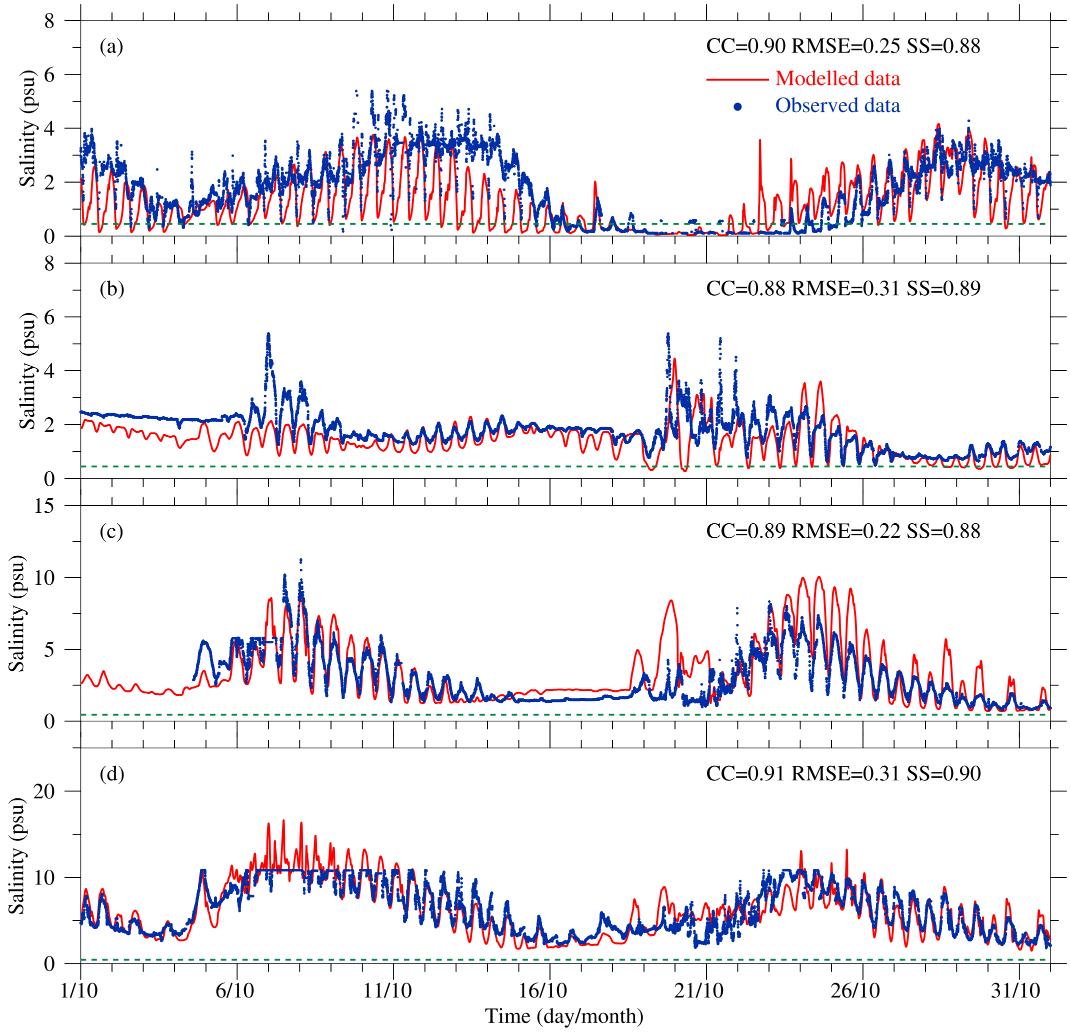

Figure 4. Daily distribution of salinity at hydrological stations in October, 2022. (a) Chongxi; (b) Nanmen; (c) Baozhen and (d) Hengshabei.

observed during mid-tides (Figures 4b–4d). At the Nanmen station, salinity was influenced by both SSO and direct saltwater intrusion, with a greater contribution from SSO. Northerly winds facilitated saltwater transport into the estuary, leading to significant increases in observed salinity at these stations on 4 and 22 October (Figures 2c and 2d). However, during the period of strong northerly winds from 6 to 20 October, salinity increased only slightly, and a marked decline was recorded on 20 October. This reduction was attributed to the emergency water release from the TGR on 2 October (Figure 2a).

The numerical model demonstrates strong agreement with observed salinity data across the stations, as reflected by high CC, low RMSE, and SS close to 1. At the Chongxi station, the model captures the semi-diurnal fluctuations in salinity and their timing accurately, achieving a CC of 0.9, RMSE of 0.25 psu, and SS of 0.88. Similar performance is observed at the Nanmen, Baozhen and Hengshabei stations, with CC greater than 0.88, RMSE less than 0.31 psu, and SS greater than 0.88, and the model reproduced the main salinity trends during the simulation period. In early October, we observed that the simulated salinity at Chongxi and Nanmen stations is lower than the measured values. The salinity at these two stations is mainly controlled by SSO, and the selection of bottom drag coefficient is critical for accurately simulating SSO (Lyu & Zhu, 2018). The bottom drag coefficient was calibrated using long-term salinity records at the Chongxi and Nanmen stations and updated bathymetric data from 2021. This parameterization yields an overall satisfactory agreement with observed salinity distributions. While the SSO process is sensitive to the bottom friction, especially in localized areas near bifurcations, its influence on the overall salinity

19447973, 2025, 8, Downloaded from https://agupubs.onlinelibrary.wiley.com/doi/10.1029/2025WR040033 by Carlo Gualtieri - Uni Federico Ii Di Napoli , Wiley Online Library on [18/08/2025]. See the Terms and Conditions (https://onlinelibrary.wiley.com/terms-and-conditions) on Wiley Online Library for rules of use; OA articles are governed by the applicable Creative Commons License

Table 1
Summary of Numerical Experiment Setup

Experiment	Emergency freshwater release	Cold fronts	Purpose
Exp. 1	Yes	Yes	Baseline scenario
Exp. 2	No	Yes	Effect of removing freshwater release
Exp. 3	Yes	No	Effect of removing cold fronts

distribution during the cold front event is minor. In this scenario, the dominant saline input originated from direct intrusion from the NC, any local error does not materially affect the main conclusions of the study.

The model's statistical performance metrics and its ability to replicate the overall temporal and spatial trends of salinity confirm its reliability. The model is well-suited for simulating the extreme saltwater intrusion event and analyzing the impacts of emergency freshwater release operations and cold fronts on estuarine dynamics.

2.3. Numerical Experiment

A background experiment (Exp. 1) was initially configured in this study, incorporating actual runoff conditions and cold front scenarios. To assess the impact of the emergency freshwater release, a comparative experiment (Exp. 2) without release was conducted, with October runoff fixed at 10,000 m^3/s. To decouple the effects of cold fronts, an additional comparative experiment was conducted (Exp. 3), substituting strong northerly winds during two cold front (October 15–20 and October 22–25) events with a 4 m/s northeasterly wind. This "climatological wind" was derived from analysis of hourly wind data recorded at the Weather Station (location shown in Figure 1) over the period 2007–October 2022. October wind records from each year were extracted and averaged under non-frontal conditions. The analysis (Figure 14) revealed that northeasterly winds dominate during October, with an average speed of approximately 4 m/s, which was used to represent typical background wind forcing in Exp. 3. The numerical experiments are summarized in Table 1.

2.4. Analytical Method

To quantify tidal asymmetry and gravitational circulation, the residual current and vertical velocity shear are defined as follows:

$$\overrightarrow{Vr} = \frac{1}{T}\int_0^T u_{(t)} d_t, \tag{2}$$

$$\mathrm{VS} = \left(\frac{\partial \mathrm{u}}{\partial \mathrm{z}}\right)^2 + \left(\frac{\partial \mathrm{v}}{\partial \mathrm{z}}\right)^2, \tag{3}$$

Where $\overrightarrow{Vr}$ represents the residual current, T is the time-averaging period (six tidal cycles, approximately 3 days in this study), and $u_{(t)}$ denotes to the velocity at a specified cross-section. The term VS indicates the vertical velocity shear, with z representing the depth, u denoting the eastward velocity, and v the northward velocity.

To identify horizontal water flux transport, the unit width net transport (UWNT) of water is defined as:

$$\overrightarrow{\mathrm{Tr}} = \frac{1}{T}\int_0^T \int_{-1}^0 (h+\xi)\vec{V} d\sigma dt, \tag{4}$$

where T is the time-averaged period (six tidal cycles, approximately 3 days in this study), h is the water depth, ξ is the water surface elevation, $\vec{V}$ is the velocity vector, and σ is the relative depth (0 at the surface and -1 at the bottom).

The net cross-sectional water flux is expressed as:

19447973, 2025, 8, Downloaded from https://agupubs.onlinelibrary.wiley.com/doi/10.1029/2025WR040033 by Carlo Gualtieri - Uni Federico Ii Di Napoli , Wiley Online Library on [18/08/2025]. See the Terms and Conditions (https://onlinelibrary.wiley.com/terms-and-conditions) on Wiley Online Library for rules of use; OA articles are governed by the applicable Creative Commons License

$$F_q = \left\langle \iint udA \right\rangle = \left\langle \int_0^L \int_{-1}^0 (h+\xi)\, ud\sigma dy \right\rangle, \tag{5}$$

where ⟨⟩ represents time averaging (implemented via 36-hr low-pass filtering), A is the tidally varying cross-sectional area, dA is the differential of A, L is the width of the cross-section, and u is the velocity perpendicular to the cross-section.

The total net cross-sectional salt flux is defined as:

$$F_s = \left\langle \iint uSdA \right\rangle = \left\langle \int_0^L \int_{-1}^0 (h+\xi)\, uSd\sigma dy \right\rangle, \tag{6}$$

where S represents salinity. To disentangle the mechanisms driving the total salt flux in the Changjiang River estuary, the velocity is decomposed into three components (Lerczak et al., 2006):

$$u_0(t) = \frac{1}{A_0}\left\langle \iint u(y,\sigma,t)\, d_A \right\rangle = \frac{1}{A_0}\left\langle \int_0^L \int_{-1}^0 (h+\xi)\, ud_\sigma d_y \right\rangle, \tag{7}$$

$$u_e(y,\sigma,t) = \frac{\langle ud_A \rangle}{\langle d_A \rangle} - u_0(t), \tag{8}$$

$$u_t(y,\sigma,t) = \mathrm{u} - u_e(y,\sigma,t) - u_0(t), \tag{9}$$

where A_0 is the low-pass cross-sectional area. The first component, u_0, is the tidally and cross-sectionally averaged velocity. The second, u_e, is the tidally averaged but cross-sectionally varying velocity, reflecting the vertical flow structure. The third, u_t, captures the tidally and cross-sectionally varying velocity. Salinity (S) can similarly be decomposed into three corresponding components.

Thus, the total cross-sectional salt flux is expressed as:

$$\begin{aligned} F_s &= \left\langle \int_0^L \int_{-1}^0 (h+\xi)\, uSd_\sigma d_y \right\rangle, \\ &= \left\langle \int_0^L \int_{-1}^0 (h+\xi)(u_0+u_e+u_t)(S_0+S_e+S_t)\, d_\sigma d_y \right\rangle, \\ &= \left\langle \int_0^L \int_{-1}^0 (h+\xi)(u_0S_0+u_eS_e+u_tS_t+\text{residual terms})\, d_\sigma d_y \right\rangle, \\ &\approx \left\langle \int_0^L \int_{-1}^0 (h+\xi)(u_0S_0+u_eS_e+u_tS_t)\, d_\sigma d_y \right\rangle, \\ &= Q_0S_0 + F_e + F_t. \end{aligned} \tag{10}$$

Here, Q_0S_0 represents the advective salt flux driven by river discharge and wind-induced flows. F_e denotes the steady shear dispersion flux controlled by estuarine circulation, while F_t represents the tidal oscillatory salt flux caused by time correlations between u and S across the cross-sectional area. Residual terms, generally negligible, are excluded from the analysis (Lerczak et al., 2006).

3. Results

3.1. Effects of Emergency Freshwater Release

The emergency freshwater release implemented during the extreme drought in the Changjiang River Estuary had pivotal effects on mitigating saltwater intrusion. Figure 5 illustrates the average salinity distribution from October 19 to 21 during a neap tide. Without the freshwater release, the surface salinity distribution (Figure 5a) reveals that

19447973, 2025, 8, Downloaded from https://agupubs.onlinelibrary.wiley.com/doi/10.1029/2025WR040033 by Carlo Gualtieri - Uni Federico Ii Di Napoli , Wiley Online Library on [18/08/2025]. See the Terms and Conditions (https://onlinelibrary.wiley.com/terms-and-conditions) on Wiley Online Library for rules of use; OA articles are governed by the applicable Creative Commons License

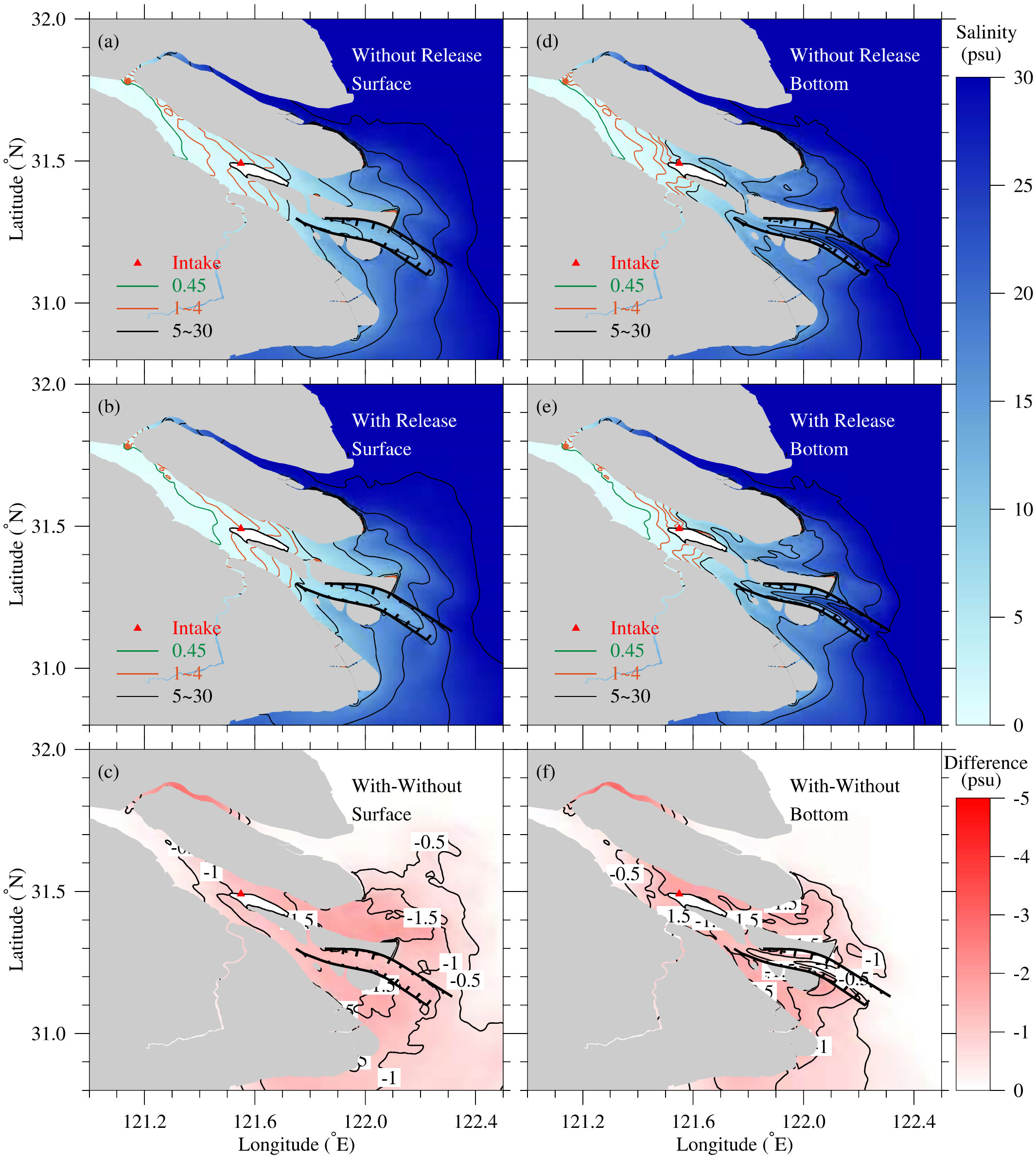

Figure 5. Tidal-averaged salinity distribution from 19 to 21 October 2022, comparing conditions with and without the emergency freshwater release. (a) Surface salinity without emergency freshwater release; (b) Surface salinity with emergency freshwater release; (c) Surface salinity difference between with and without release; (d) Bottom salinity without emergency freshwater release; (e) Bottom salinity with emergency freshwater release; (f) Bottom salinity difference between with and without release.

the NB is dominated by high-salinity water. Specifically, the salinity reached 4 psu at the NB entrance and increased to 25 psu in the middle. This phenomenon can be attributed to the funnel-shaped geometry of the NB, which amplifies the tidal range while reducing river discharge inflow due to the narrower tidal flat in the upper reaches (H. Wu et al., 2006). Water with salinity exceeding 1 psu intruded into the upper reaches of the SB, primarily driven by saltwater spillover (SSO) from the NB. The combined effects of the SSO and direct saltwater intrusion from the NC resulted in an overall high-low-high salinity distribution pattern in the SB. High-salinity water also entered NC through its northern outlet (Li et al., 2014), forming a distinct salinity front. Salinity levels within this front measured 18 psu, dropping to 3 psu in the middle and 1.5 psu near the water intake of the QCSR. A river plume extended northeastward from the northern side of the NC, while salinity levels in the SC ranged between 1and 3 psu. In the NP, freshwater flowed into the East China Sea along the deep waterway project, extending southward under the influence of the Coriolis force. Meanwhile, a landward salinity front developed in

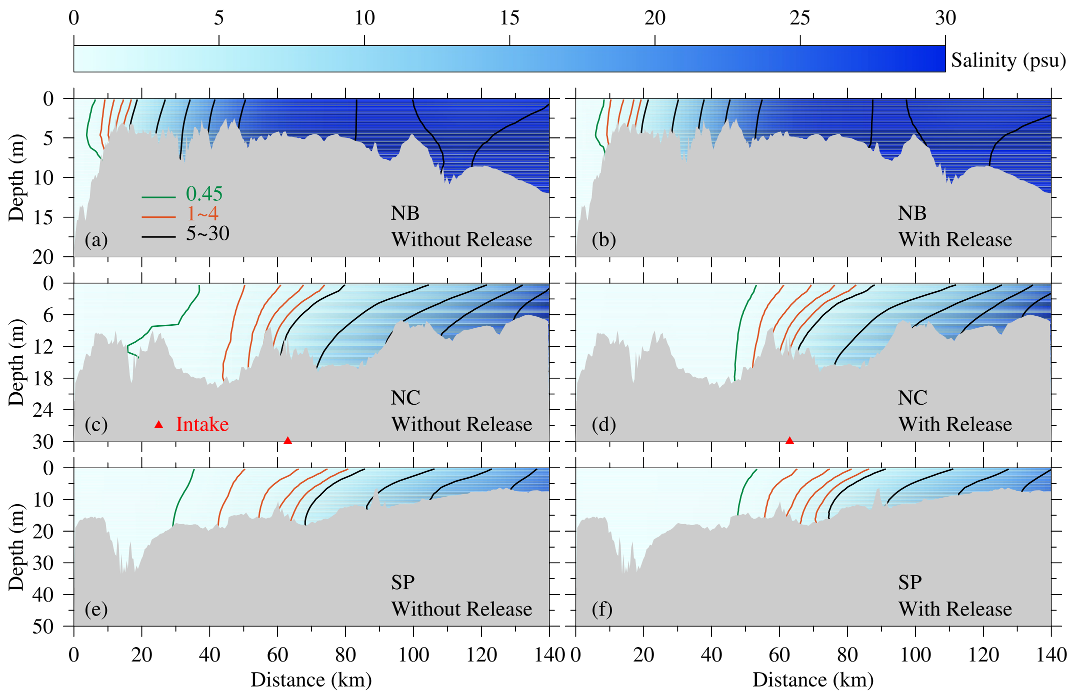

Figure 6. Longitudinal distribution of tidal-averaged salinity from 19 to 21 October 2022, comparing conditions with and without emergency freshwater release. (a) North Branch (NB) salinity without emergency freshwater release; (b) NB salinity with emergency freshwater release; (c) North Channel (NC) salinity without emergency freshwater release; (d) NC salinity with emergency freshwater release; (e) South Passage (SP) salinity without emergency freshwater release; (f) SP salinity with emergency freshwater release.

the SP, driven by landward subtidal transport caused by tidal interactions with shallow topography (H. Wu et al., 2010). Without the freshwater release, the isohalines moved downstream, and a large freshwater area emerged in the SB (Figure 5b), where salinity near the intake decreases to 1 psu. Surface salinity in the middle of the NB and sandbar areas significantly decreased of approximately 2 psu (Figure 5c). Without the freshwater release, the bottom salinity distribution revealed a landward-intruding high-salinity front caused by the classic estuarine circulation, which leads to denser isohalines (Figure 5d). In the NP and SP, the bottom isohalines display a trend opposite to that of the surface isohalines, influenced by baroclinic forces. Without the freshwater release, the position of the salinity front in the bottom layer remained largely unchanged (Figure 5e). The bottom salinity had only a slight decrease lower than 1.5 psu (Figure 5f), with the affected area confined to the estuary. Overall, the freshwater release significantly reduces salinity levels in the Changjiang River Estuary, weakening both the SSO from the NB and the direct saltwater intrusion from the NC. The magnitude and range of salinity reduction were notably larger at the surface than at the bottom. The more significant reduction in surface salinity compared to bottom salinity can be attributed to vertical stratification during cold front conditions. Strong northerly winds induced a wind-driven horizontal circulation pattern which further reinforced stratification by maintaining a sharp vertical salinity gradient and limiting the downward mixing of freshwater. The buoyant freshwater propagated along the surface, while denser saline water remained at bottom. Although some vertical mixing occurred, it was insufficient to fully erode the stratification.

Section P1 is located along the NB. The upper reaches of the NB are almost perpendicular to the SB, while the lower and middle reaches exhibit a funnel-like shape. This unique morphology inhibits runoff from flowing into the NB, resulting in a larger tidal range within it. Due to the shallow topography, the salinity along section P1 was well-mixed vertically, with the isohalines displaying nearly vertical homogeneity. Without the freshwater release, the salinity front was located in the middle and upper reaches (5–45 km) of the NB (Figure 6a). Following the emergency freshwater release, the salinity remains relatively unchanged due to only a slight increase in runoff entering the NB (Figure 6b). Section P2 is aligned along the SB and NC. The NC acts as the major outlet for runoff into the ocean. The isohalines slope downstream due to amount of freshwater entering the NC, which lowers the surface salinity (Figure 6c). A classical gravitational circulation was observed in the NC, as the freshwater moves

19447973, 2025, 8, Downloaded from https://agupubs.onlinelibrary.wiley.com/doi/10.1029/2025WR040033 by Carlo Gualtieri - Uni Federico Ii Di Napoli , Wiley Online Library on [18/08/2025]. See the Terms and Conditions (https://onlinelibrary.wiley.com/terms-and-conditions) on Wiley Online Library for rules of use; OA articles are governed by the applicable Creative Commons License

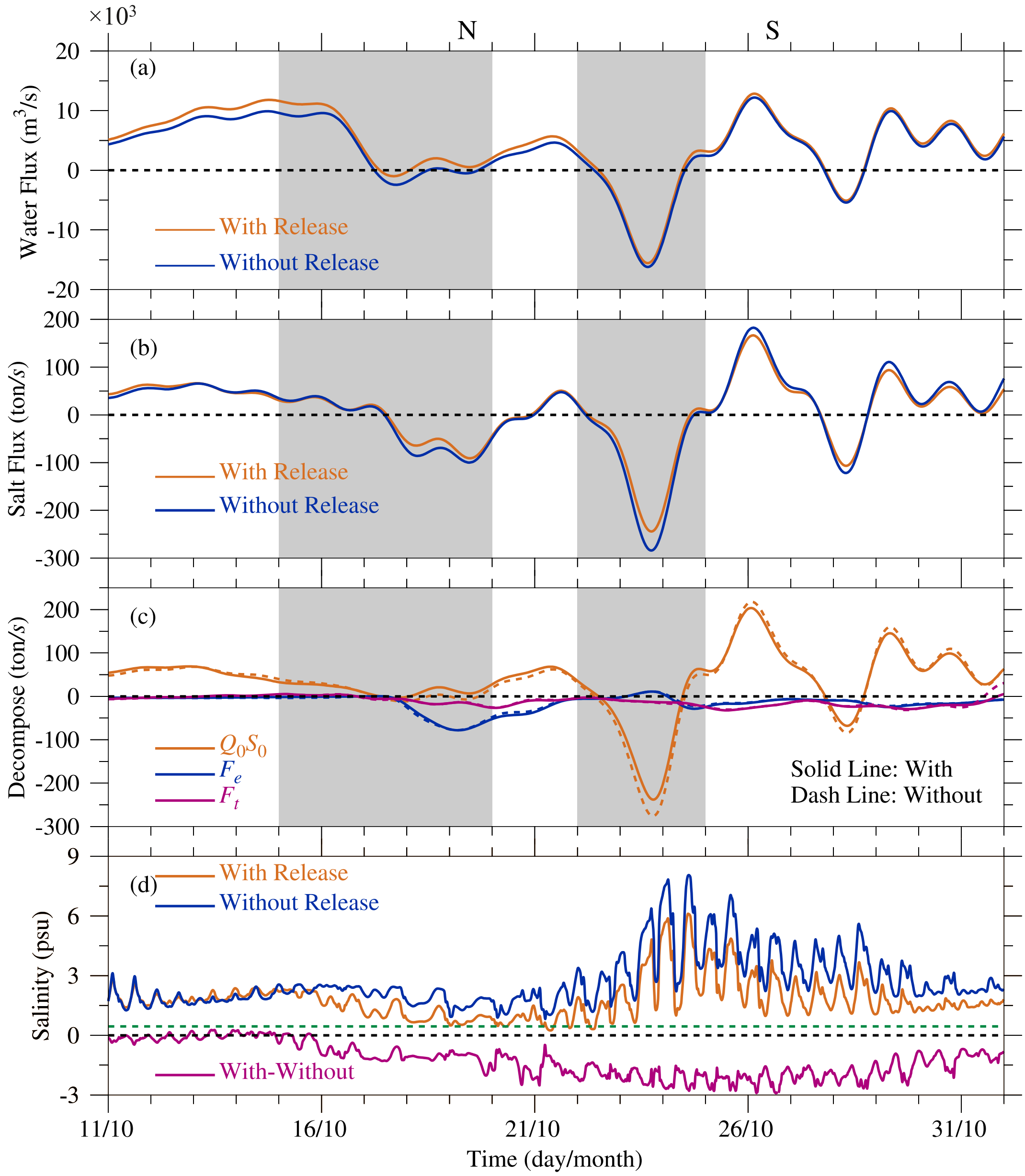

Figure 7. Daily distribution of water fluxes (a), salt fluxes (b), salt flux decomposition (c) across section Sec1, and salinity (d) at the QCSR intake from 11 to 31 October 2022, under conditions with and without freshwater release. N and S represent neap tide and spring tide, respectively. Positive values indicate seaward flux, while negative values indicate landward flux. The green dashed line represents the 0.45 psu (same below).

seaward at the surface while saline water moved landward at the bottom, driven by the baroclinic pressure gradient force. Stratification level increased toward the ocean, and the water columns maintained a steady stratification state in the lower reaches of the NC (65–140 km). After freshwater release (Figure 6d), the freshwater input increased, and the isohalines shift seaward. The 0.45 psu isohaline moves seaward by ~17 km, and the salinity dropped below 1 psu near the QCSR. Section P3 is located along the SB and SC. This section had a more inclined distribution of isohalines, resulting in a more pronounced vertical salinity stratification (Figure 6e). After the freshwater release (Figure 6f), the isohalines along P3 shifted downstream, and the 0.45 psu isohaline moved seaward by ~19 km.

The NC serves as the major channel of the Changjiang River to the sea. Prior to the emergency freshwater release, the water flux across the Sec1 was predominantly seaward, consistent with the river's natural flow direction

19447973, 2025, 8, Downloaded from https://agupubs.onlinelibrary.wiley.com/doi/10.1029/2025WR040033 by Carlo Gualtieri - Uni Federico Ii Di Napoli , Wiley Online Library on [18/08/2025]. See the Terms and Conditions (https://onlinelibrary.wiley.com/terms-and-conditions) on Wiley Online Library for rules of use; OA articles are governed by the applicable Creative Commons License

19447973, 2025, 8, Downloaded from https://agupubs.onlinelibrary.wiley.com/doi/10.1029/2025WR040033 by Carlo Gualtieri - Uni Federico Ii Di Napoli , Wiley Online Library on [18/08/2025]. See the Terms and Conditions (https://onlinelibrary.wiley.com/terms-and-conditions) on Wiley Online Library for rules of use; OA articles are governed by the applicable Creative Commons License

(Figure 7a). However, during the two cold front events, significant landward water flux was observed. Following the release, river discharge increased, enhancing the seaward water flux through transect Sec2, with a peak increase of 1,687 m^3/s on October 18. As salt moved with water, changes in salt flux mirrored those in water flux (Figure 7b). Notably, during the two cold front events, landward salt flux was observed through transect Sec2. After the freshwater release, the maximum reduction in landward salt flux reaches 20 ton/s on October 18, indicating that the emergency freshwater release mitigated the upstream intrusion of saline water in the NC.

Decomposition of salt flux reveals that during the first cold front event, steady shear dispersion salt flux dominated the landward salt transport, with a peak value of 78 ton/s (Figure 7c). In contrast, advective transport was the primary mechanism during the second cold front, with the advective salt flux peaking at −239 ton/s (Figure 7c). This difference is attributed to the first cold front coinciding with a neap tide period, characterized by weaker tidal forces. Enhanced vertical velocity shear and salinity stratification during this period amplified landward shear salt transport. After the freshwater release, the increased river discharge intensified the seaward advective transport, reducing the landward salt flux. However, shear salt flux and tidal oscillatory salt flux remained largely unchanged. The salinity at the QCSR intake provided the clearest evidence of the emergency freshwater release's effectiveness. Post-release, salinity at the intake decreased to approximately 0.45 psu on October 21, extending the intake's usable water window by 12.75 hr (Figure 7d). However, the magnitude of salinity reduction was significantly lower than expected. This discrepancy is hypothesized to result from the cold front weakening the effectiveness of the emergency freshwater release, which will be analyzed in the next section.

3.2. Impacts of Cold Fronts

The UWNT of water, as defined in Equation 4, flows southward along the coast under the influence of northerly winds during cold fronts. However, this southward flow is obstructed by the deep waterway project, which acts as a physical barrier. The obstruction causes water to pile up in upstream areas, leading to increased residual elevation (Li et al., 2020). This wind-driven accumulation intensified landward fluxes (Figure 8a). Under cold front conditions (Figure 8b), the UWNT arrows demonstrate disrupted seaward water flow patterns compared to non-cold front conditions. Cold fronts significantly reduced water transport from the NC to the ocean, while increasing seaward transport from the SC. This differential flow created a horizontal circulation system: saline water is drawn landward into the estuary through the NC and exits seaward via the SC. Figure 8c isolates the impact of cold fronts, highlighting residual elevation differences that amplify landward and seaward transport asymmetries. Residual elevation increases were mostly placed in the upstream NC, reaching up to 0.3 m. Cold fronts induced a landward flux in the NC with a value of approximately −1 m^2/s, driven by wind-induced Ekman transport. In contrast, without cold fronts, the NC flux was seaward, with a value of 2 m^2/s, reflecting typical river-dominated dynamics. The cold front-induced shift resulted in a net change of −3 m^2/s in the NC, reversing the flux direction and significantly enhancing landward transport. Meanwhile, in the SC, cold fronts intensified the seaward flux, increasing it to 3 m^2/s, compared to 1 m^2/s without cold fronts-a net increase of 2 m^2/s. These changes reflect a redistribution of water fluxes within the estuary, with landward transport in the NC and enhanced seaward transport in the SC forming a horizontal circulation.

The changes in the UWNT significantly affect salinity distribution within the estuary. In the NC, cold fronts induced a landward flux of approximately −1 m^2/s, resulting in a salinity increase of 2–3 psu in upstream regions, with values reaching up to 5 psu (Figure 8d). Under non-cold front conditions, a seaward flux of 2 m^2/s limited upstream salinity to 0.45–2 psu (Figure 8e). Conversely, in the SC, cold fronts enhanced seaward flux to 3 m^2/s, reducing downstream salinity by 0.5–1 psu, with values falling below 0.45 psu. Without cold fronts, the weaker seaward flux of 1 m^2/s allowed salinity to rise to ∼2 psu in the SC. The salinity difference distribution between cold front and non-cold front scenarios (Figure 8f) highlights contrasting trends in the NC and SC. In the NC, salinity increased to ∼5 psu under cold front conditions due to intensified landward transport, amplifying saltwater intrusion upstream. In contrast, the SC experienced decreased salinity (∼2 psu) driven by enhanced seaward freshwater flushing, reducing salinity levels downstream. This opposing behavior underscores the complex interplay of hydrodynamic processes in multi-channel estuaries. Cold front-induced changes in water flux redistribute salinity unevenly between channels, emphasizing the system's sensitivity to these events.

Figures 9a and 9b illustrate the tidal-averaged salinity distributions along the P2 section under conditions with and without cold fronts, respectively. Under non-cold front conditions, the saltwater front was located between 80 and 140 km, forming a distinct salt wedge. During cold front events, wind-driven Ekman transport facilitated the

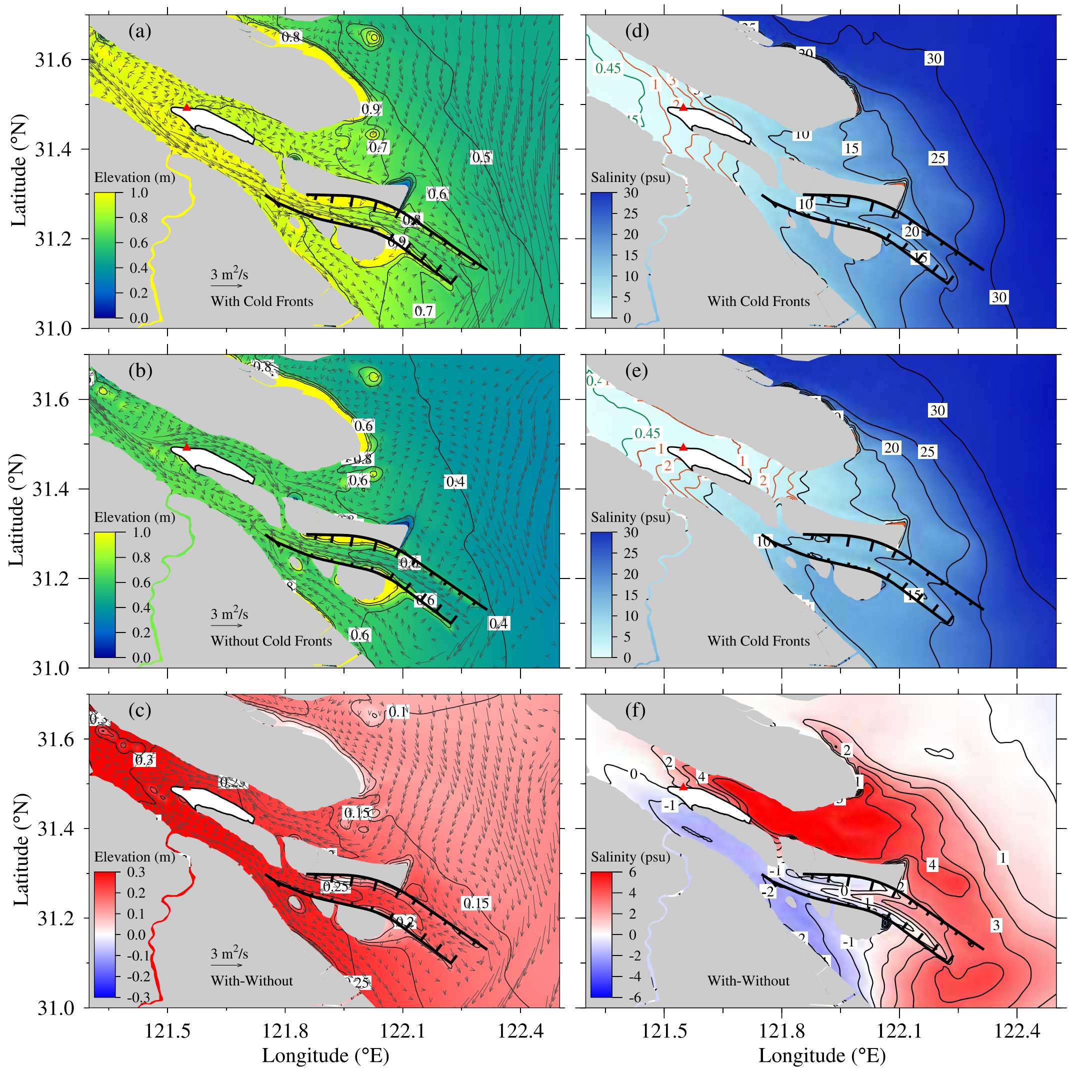

Figure 8. Spatial distribution of residual elevation, the UWNT, and vertically averaged salinity during 19–21 October 2022. Arrows indicate the UWNT. The bottom panels illustrate the differences in residual elevation and salinity between scenarios with and without cold fronts. (a) Residual elevation and the UWNT with cold fronts; (b) Residual elevation and the UWNT without cold fronts; (c) Difference in residual elevation and the UWNT (with—without cold fronts); (d) Salinity distribution with cold fronts; (e) Salinity distribution without cold fronts; (f) Difference in salinity distribution (with—without cold fronts).

landward intrusion of seawater along the bottom layer, pushing the saltwater front upstream. The 1 psu isohaline advanced ~20 km inland, intensifying salinity stratification within the 50–80 km range. The tidal-averaged residual current characterizes classic estuarine circulation dynamics (Equation 2). Without cold fronts, the residual current along P2 primarily flows seaward (Figure 9c). However, in the 100–140 km range, pronounced salinity stratification created a landward-directed residual current in the bottom layer. This resulted in vertical velocity shear exceeding 2.5 (Equation 3), caused by opposing flow directions in the surface and bottom layers. Cold fronts enhanced landward transport of high-salinity water along the bottom layer, further increasing salinity stratification. This stratification generated a landward baroclinic pressure gradient force, reversing the bottom-layer residual current to a landward direction within the 65–90 km range (Figure 9d). The intensified vertical velocity shear amplified steady shear dispersion salt flux (F_e), highlighting the significant impact of cold fronts on estuarine hydrodynamics.

The salt flux decomposition method was applied to quantify the contributions of advective, steady shear dispersion, and tidal oscillatory salt fluxes under scenarios with and without cold fronts. This analysis aimed to

19447973, 2025, 8, Downloaded from https://agupubs.onlinelibrary.wiley.com/doi/10.1029/2025WR040033 by Carlo Gualtieri - Uni Federico Ii Di Napoli , Wiley Online Library on [18/08/2025]. See the Terms and Conditions (https://onlinelibrary.wiley.com/terms-and-conditions) on Wiley Online Library for rules of use; OA articles are governed by the applicable Creative Commons License

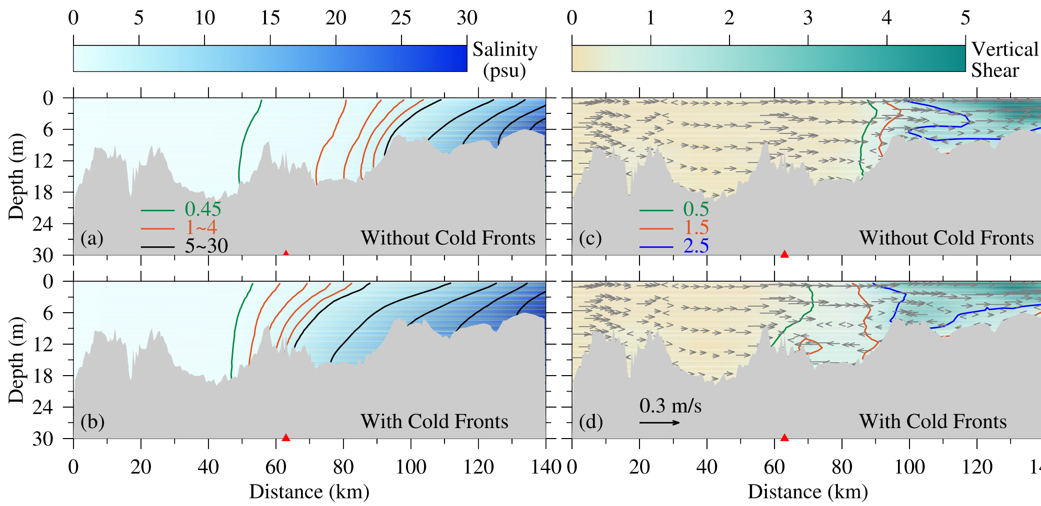

Figure 9. Tidal-averaged salinity, residual current, and vertical shear distribution along section P2 from October 19 to 21 under conditions with and without cold front events. Arrows indicate residual current.

elucidate the influence of cold fronts on estuarine dynamics and salt transport mechanisms. Figure 10a illustrates the temporal variation in water fluxes. Under non-cold front conditions, water fluxes consistently exhibited seaward transport, reflecting the dominance of river discharge. However, during cold fronts, this pattern reversed intermittently due to northerly wind-induced Ekman transport. The peak landward flux during the first cold front reached approximately −995 m^3/s, while the second cold front results in a more pronounced reversal, peaking at -15.5×10^3 m^3/s. Cold fronts disrupted typical seaward water transport by enhancing landward flows through wind-driven dynamics, which weakens freshwater release effectiveness and facilitates saltwater intrusion. Figure 10b reveals that total salt fluxes were predominantly seaward under non-cold front conditions, with peak values reaching 50 ton/s. However, during cold fronts, salt flux reversed to landward, peaking at −244 ton/s during the second event. This landward salt flux was driven primarily by wind-induced advection, overwhelming the seaward transport driven by river discharge. The magnitude of this salt flux reversal aligns closely with the intensity and duration of wind forcing.

Figure 10c depicts seaward advective transport driven by river discharge, which averages 75 ton/s on 13 October. Conversely, Figure 10d shows periodic landward advective salt flux caused by wind-induced transport, peaking at −239 ton/s during the second cold front. Steady shear dispersion flux peaked at −24 ton/s, driven by stratification and velocity shear during neap tides under non-cold front conditions. Enhanced landward F_e, peaking at −70 ton/s on 19 October, is attributed to intensified stratification resulting from reduced mixing under strong wind forcing during the first cold front. Oscillatory flux contributed approximately −10 ton/s landward under non-cold front conditions, primarily during neap tides when tidal mixing is weaker. Cold fronts significantly disrupted the balance between landward and seaward salt transport mechanisms. Wind-driven advection salt flux (Q_0S_0) played a dominant role in this disruption, leading to net landward salt transport during such events. Shear salt flux also increased during the first cold front due to enhanced vertical shear (Figure 9d), however, the change in F_e was lower than that in Q_0S_0, highlighting the predominance of wind-induced advection in the salt flux response to cold fronts. Wind-driven Ekman transport intensified landward salt flux during both cold fronts. Notably, the first cold front coincided with the freshwater release and neap tide periods, which partially offsets the landward advective flux induced by Ekman transport. As a result, the peak landward advective salt flux during the first cold front was limited to −2 ton/s, substantially lower than the −239 ton/s observed during the second cold front. This weaker landward advective flux during the first cold front underscores the potential of freshwater release operations to counteract wind-induced saltwater intrusion. However, the stark contrast with the second cold front highlights the vulnerability of such mitigation strategies to timing mismatches and intense wind events.

The SC plays a pivotal role in modulating horizontal circulation, water flux, and salt flux in the Changjiang River Estuary, underscoring a distinctive characteristic of this multi-channel estuarine system. Under the influence of cold fronts, the SC facilitated significant seaward water flux, peaking at ~13,000 m^3/s, nearly doubling the flux observed under non-cold-front conditions during the first cold front (Figure 11a). This intensified flux enhanced

19447973, 2025, 8, Downloaded from https://agupubs.onlinelibrary.wiley.com/doi/10.1029/2025WR040033 by Carlo Gualtieri - Uni Federico Ii Di Napoli , Wiley Online Library on [18/08/2025]. See the Terms and Conditions (https://onlinelibrary.wiley.com/terms-and-conditions) on Wiley Online Library for rules of use; OA articles are governed by the applicable Creative Commons License

19447973, 2025, 8, Downloaded from https://agupubs.onlinelibrary.wiley.com/doi/10.1029/2025WR040033 by Carlo Gualtieri - Uni Federico Ii Di Napoli , Wiley Online Library on [18/08/2025]. See the Terms and Conditions (https://onlinelibrary.wiley.com/terms-and-conditions) on Wiley Online Library for rules of use; OA articles are governed by the applicable Creative Commons License

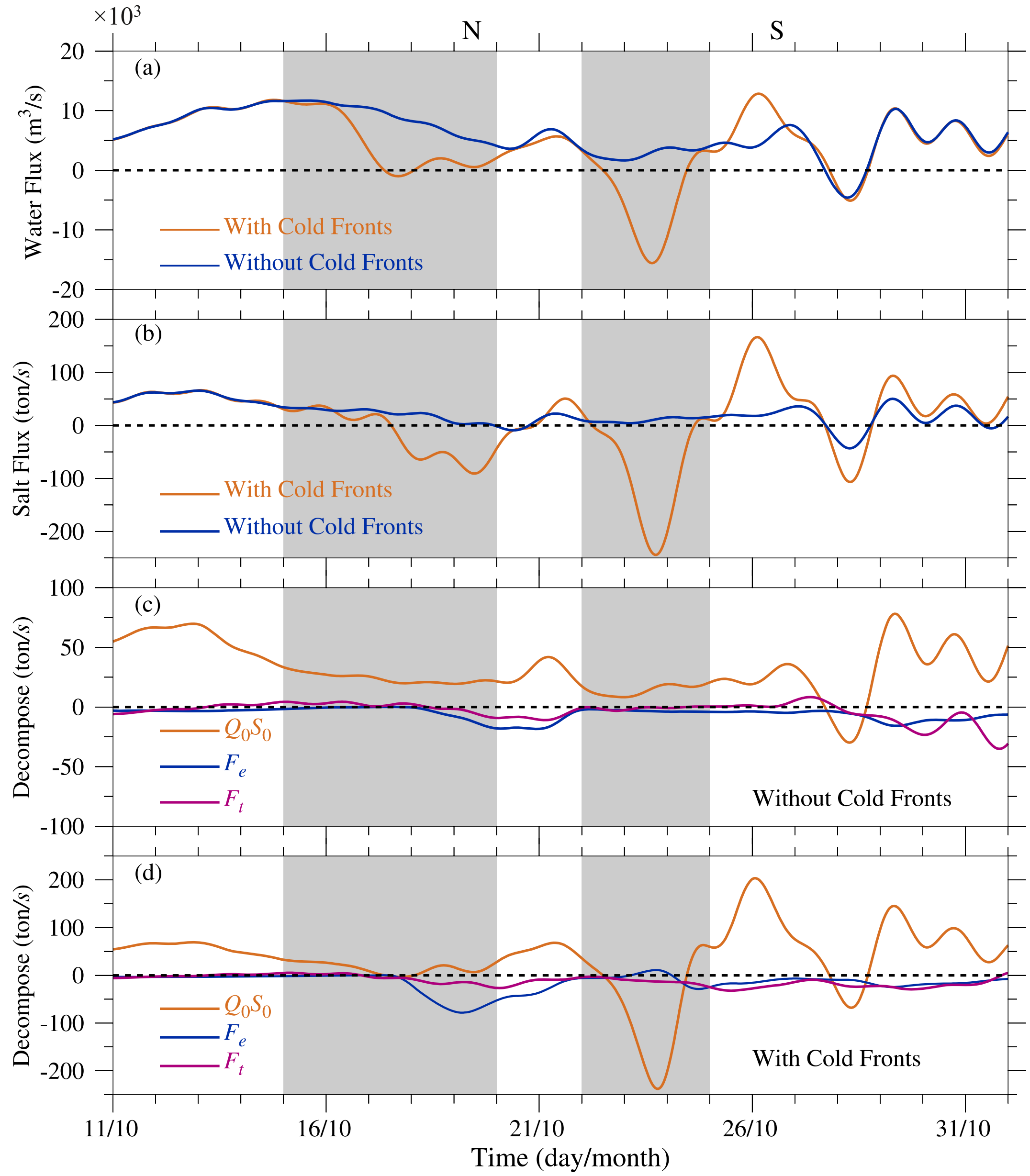

Figure 10. Daily distribution of water fluxes (a) and salt fluxes (b) across Sec1 under conditions with and without cold fronts. Panels (c) and (d) present the decomposition of total salt flux into its constituent components: advective transport (Q_0S_0), steady shear dispersion (F_e), and tidal oscillatory salt fluxes (F_t), under conditions without and with cold fronts.

horizontal circulation, wherein saline water moved landward via the NC and subsequently flushed seaward through the SC. During cold front events, the salt flux through the SC was predominantly seaward, reaching a peak of 13 ton/s. This pattern was driven by wind-induced Ekman transport, which channels saline water landward into the NC and then redirects it seaward through the SC (Figure 11b). In contrast, under non-cold-front conditions, salt flux moved landward, peaking at −12 ton/s on October 21, primarily due to subtidal transport induced by tidal interactions with the SC's shallow topography. This dual behavior highlights the dynamic function of the SC in regulating salt transport and maintaining estuarine balance, further distinguishing the Changjiang River Estuary as a globally unique multi-branch system.

The temporal variation of salinity at the water intake (Figure 11c) highlights the distinct influence of cold fronts on salinity dynamics and freshwater intake period. During the first cold front, the emergency freshwater release successfully reduced salinity at the intake; however, salinity remained at ~0.45 psu, rendering the water

19447973, 2025, 8, Downloaded from https://agupubs.onlinelibrary.wiley.com/doi/10.1029/2025WR040033 by Carlo Gualtieri - Uni Federico Ii Di Napoli , Wiley Online Library on [18/08/2025]. See the Terms and Conditions (https://onlinelibrary.wiley.com/terms-and-conditions) on Wiley Online Library for rules of use; OA articles are governed by the applicable Creative Commons License

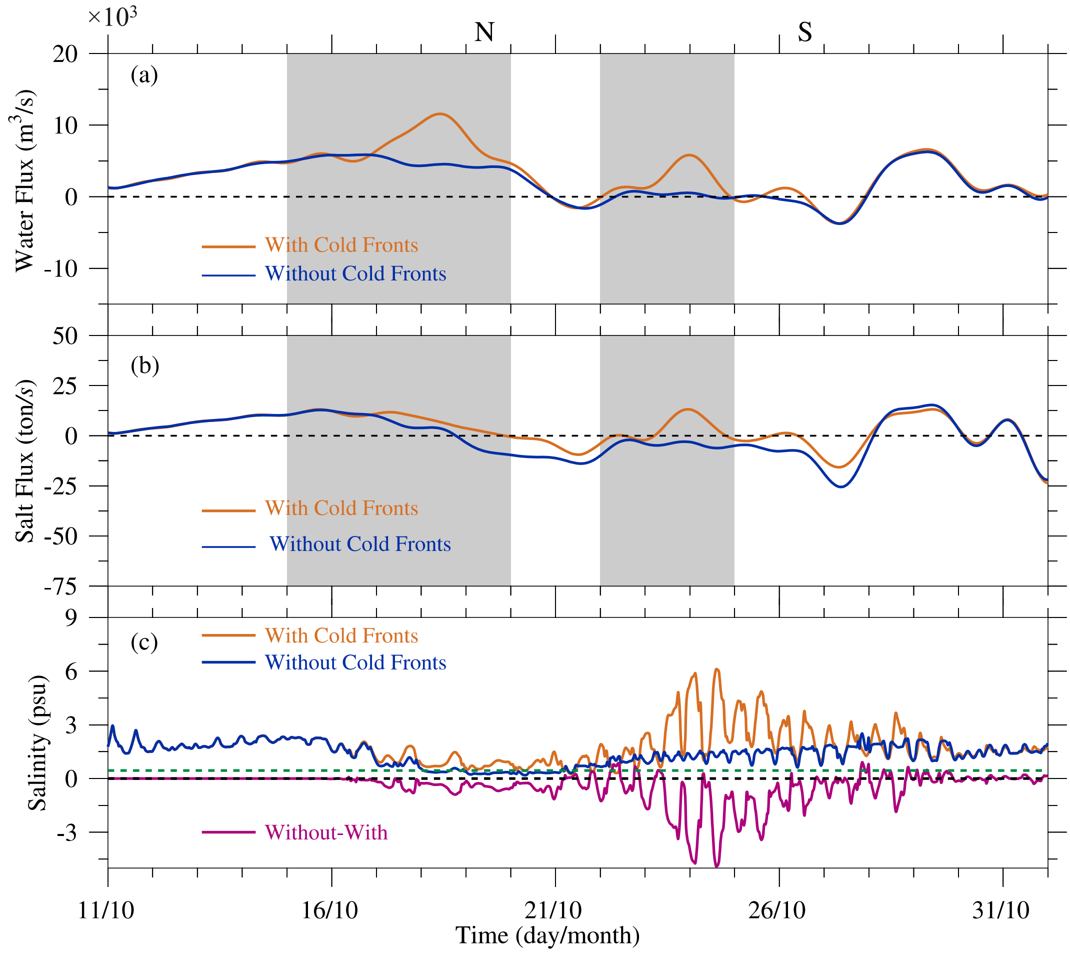

Figure 11. Daily distribution of water fluxes (a) and salt fluxes (b) across Sec2 and salinity at the intake of the QCSR (c) under various scenarios.

unsuitable for intake. In contrast, under non-cold-front conditions, salinity levels would have decreased below 0.45 psu, significantly improving freshwater intake conditions. This improvement would have extended the QCSR's freshwater intake window from 12.75 to 36.89 hr (Table 2), substantially enhancing the operational timeframe for water intake activities. These findings emphasize the adverse effects of cold fronts on the effectiveness of emergency freshwater release and underscore the necessity of optimizing freshwater release timing from upstream reservoirs to maximize reservoir intake opportunities in the Changjiang River Estuary.

4. Discussion

4.1. Sensitivity Analysis on Freshwater Release Timing

Extensive research has demonstrated that saltwater intrusion significantly threatens freshwater resource management in estuaries and delta regions worldwide. Increasing river discharge through reservoir operations is a reasonable measure to mitigate estuarine saltwater intrusion. To maximize the effectiveness of such operation, it is essential to synchronize the arrival of increased water volume at the estuary with periods of minimal salinity. In tidal estuaries, tidal dynamics are most intense during spring tides, exacerbating seawater intrusion. Consequently, delivering supplemental water during neap tides can substantially enhance its impact.

Table 2
Water Intake Periods at the QCSR With and Without Cold Fronts

Scenario	Water intake period (hours)
With cold fronts	12.75
Without cold fronts No. 1, 2	36.89

The Changjiang River Estuary is a typical tidal estuary, where optimizing freshwater release effectiveness necessitates accurately calculating the

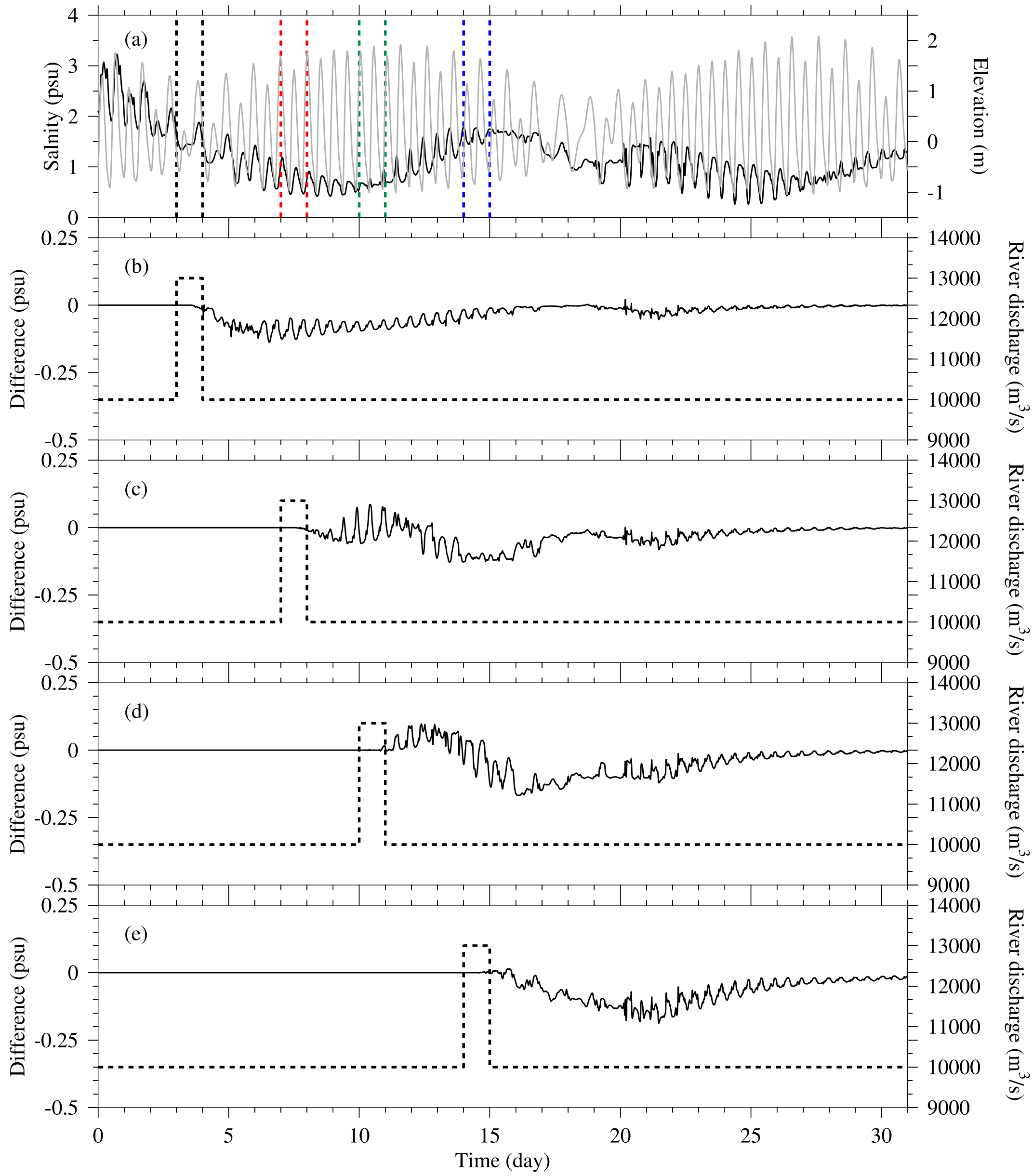

Figure 12. Daily distribution of salinity for the increased river discharge during different tide type. (a) Temporal variation of salinity and tidal elevation at the intake location; (b) Salinity difference after the discharge increase during neap tide; (c) Salinity difference after the discharge increase during the mid-tide following neap tide; (d) Salinity difference after the discharge increase during spring tide; (e) Salinity difference after the discharge increase during the mid-tide following spring tide.

salinity response time at the QCSR intake following changes in river discharge. To address this, four experiments were conducted to analyze salinity variations at the QCSR intake. In these experiments, river discharge was increased by 3,000 m^3/s for 1 day under four distinct tidal conditions: neap tide, mid-tide following neap tide, spring tide, and mid-tide following spring tide (Figure 12a).

The results indicate that increasing river discharge during neap tide caused salinity at the QCSR intake to begin fluctuating approximately 15 hr later. The maximum salinity reduction was observed 4.0 days after the discharge increase, stabilizing at a decrease of approximately 0.12 for 1.5 days (Figure 12b). These changes propagated through the estuary via advection and wave mechanisms. The propagation time of shallow water waves to the Changjiang River was previously estimated to be 15.1 hr (Yuan et al., 2016), aligning closely with the observed

19447973, 2025, 8, Downloaded from https://agupubs.onlinelibrary.wiley.com/doi/10.1029/2025WR040033 by Carlo Gualtieri - Uni Federico Ii Di Napoli , Wiley Online Library on [18/08/2025]. See the Terms and Conditions (https://onlinelibrary.wiley.com/terms-and-conditions) on Wiley Online Library for rules of use; OA articles are governed by the applicable Creative Commons License

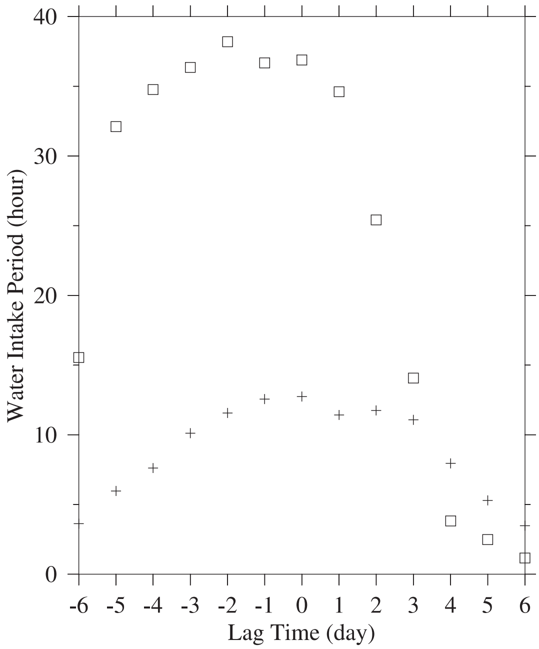

Figure 13. Water intake period corresponds to the lag time for scenarios with or without cold fronts, Plus: with cold fronts, Box: without cold fronts.

salinity response time at the water intake. However, nonlinear tidal effects and bottom drag may introduce variations.

When river discharge increased during mid-tide after neap tide, salinity fluctuations at the water intake began approximately 17 hr later. The maximum salinity reduction was observed after 7.0 days, stabilizing at a decrease of approximately 0.1 for 2 days (Figure 12c). Conversely, increasing discharge during spring tide results in salinity fluctuations beginning after 20 hr, with the maximum reduction occurring 6.0 days later and stabilizing around 0.17 for 1 day (Figure 12d). Finally, when discharge increased during mid-tide after spring tide, salinity fluctuated after 18 hr, with the maximum reduction observed after 7.5 days, stabilizing around 0.2 for 1.5 days (Figure 12e).

In summary, salinity at the QCSR intake responds to changes in discharge after an average of 17.5 hr. The maximum salinity reduction was observed after 6.1 days in average, with the specific timing and magnitude of the response varying according to the tidal phase. During neap tides, weaker tidal forcing led to stronger vertical stratification. The released freshwater remained concentrated in the surface layer and propagate more rapidly downstream, resulting in the fastest salinity response at the intake. In contrast, stronger tidal currents during spring tides enhanced vertical mixing, dispersing freshwater and delaying its influence at the intake.

In practical release operation, river discharge increases are typically continuous and sustained over extended periods. To assess the impact of emergency release timing, two additional sets of numerical experiments were conducted based on both EXP.1 and EXP.3 as baseline scenarios. In these experiments, the total volume of freshwater release was held constant while only the timing was varied. One group of experiments was performed under cold front conditions, while the other group excluded the cold front, allowing for a comparative analysis of how timing influences the effectiveness of freshwater intrusion suppression. The results demonstrate that the timing of the release significantly influences water intake period.

Under conditions with cold fronts, the longest water intake period was observed for the original release timing, with a period of 12.75 hr. Conversely, under conditions without cold fronts, the longest water intake period was found when the release started 2 days earlier, reaching 38.20 hr (Figure 13).

4.2. Influence of Wind Direction

Historical wind speed data from the Weather Station (Figure 1) were compiled for the period from 2007 to October 2022. This analysis revealed that the dominant wind direction in October is northeasterly (Figure 14). Given this prevailing wind pattern, its impact on saltwater intrusion in the Changjiang River Estuary warrants discussion. Northeasterly winds, which drive downstream movement, are likely to influence estuarine circulation and salinity distribution, potentially exacerbating saltwater intrusion. Such an analysis is critical for understanding the mechanisms underlying salt transport during this period and for proposing effective freshwater release strategies.

Experimental results indicate that when wind speed remains constant and wind direction aligns with the dominant northeasterly winds in October, the water flux across Sec1 is consistently transported seaward, even during cold front events (Figure 15a). Correspondingly, the salt flux through Sec1 also shifted seaward. As the wind direction shifted from northerly to northeasterly, the maximum landward salt flux across Sec1 significantly decreased, from 241 to 11 ton/s (Figure 15b). Salt flux decomposition further reveals that all component fluxes were substantially weakened under northeasterly wind. The most notable change was observed in the advective salt flux, which decreased from a landward value of 239 ton/s to a net seaward transport (Figure 15d). This result clearly highlights the critical role of wind direction in regulating salt transport through the North Channel. Consequently, under the influence of northeasterly winds, salinity at the QCSR intake decreases substantially, stabilizing around 0.45 from October 19 to 23 (Figure 15d), which is favorable for freshwater resource utilization.

19447973, 2025, 8, Downloaded from https://agupubs.onlinelibrary.wiley.com/doi/10.1029/2025WR040033 by Carlo Gualtieri - Uni Federico Ii Di Napoli , Wiley Online Library on [18/08/2025]. See the Terms and Conditions (https://onlinelibrary.wiley.com/terms-and-conditions) on Wiley Online Library for rules of use; OA articles are governed by the applicable Creative Commons License

10.1029/2025WR040033

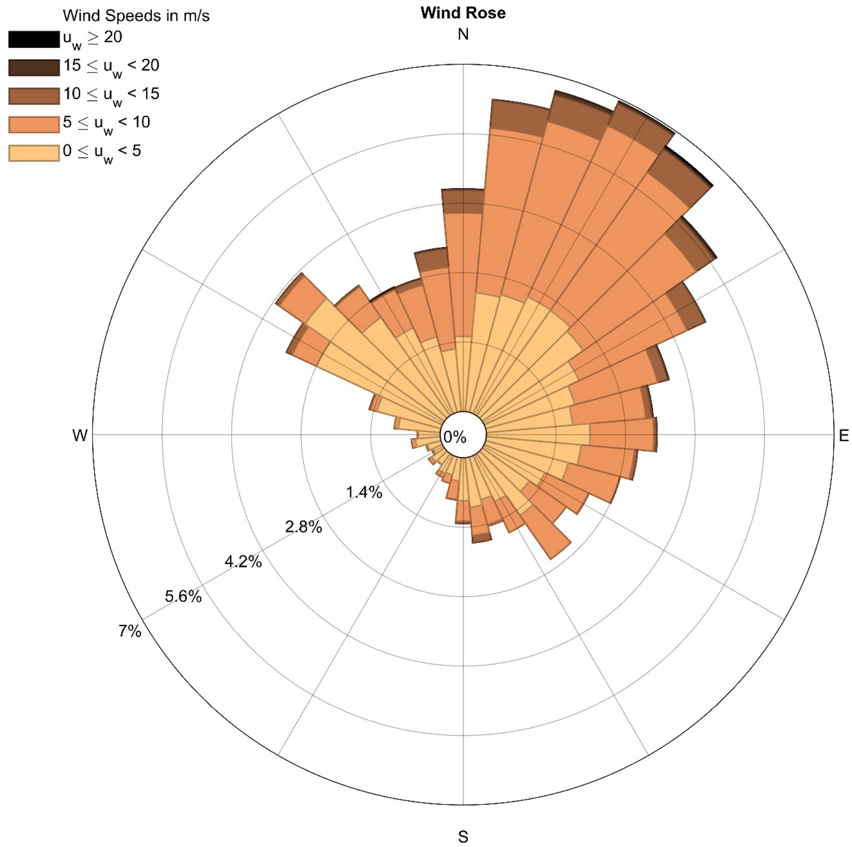

Figure 14. Analysis of historical wind speed data (2007–October 2022) from the Weather Station reveals that northeasterly winds dominate in October.

4.3. Distinctive Features and Future Directions

Cold fronts significantly affected saltwater intrusion dynamics and the effectiveness of emergency freshwater release operations in the Changjiang River Estuary. H. Wu et al. (2010) simulated horizontal estuarine circulation driven exclusively by northerly winds, revealing seawater intrusion via the NC and outflow through the SC. Li et al. (2012) examined the influence of wind speed and direction on the SSO, reporting that at a wind speed of 5 m/s, northerly winds caused the most severe SSO, followed by northwesterly winds, with northeasterly winds exerting the weakest impact. Zhang et al. (2019) demonstrated that frequent strong northerly wind events during winter elevate water levels in the northern branch, intensifying the SSO, with wind-induced Ekman transport identified as the primary driving mechanism. Building on these studies, our findings highlight the complex interplay between emergency freshwater release operations and meteorological events in mitigating saltwater intrusion in the Changjiang River Estuary.

In the context of climate change and the increasing frequency of extreme weather events, this study faces certain limitations. First, the simulations were based on a specific set of hydrological and meteorological conditions, which may not capture the full range of variability in the Changjiang River Estuary. Second, the findings are specific to the Changjiang River Estuary and may require adaptation to be applicable to other estuarine systems with differing morphological and hydrodynamic characteristics.

Future research should investigate the scalability of these findings to other estuarine systems worldwide, particularly those with multi-channel configurations. For example, the Mekong Estuary, a highly vulnerable and sensitive tidal system, is experiencing intensified saltwater intrusion driven by sea-level rise, extreme droughts, and upstream regulation (Eslami et al., 2021). The extensive network of upstream reservoirs in the Mekong basin further highlights the urgency of developing cross-border freshwater management strategies. Despite differences in scale and setting, the Changjiang and Mekong estuaries share key hydrodynamic and morphological features.

19447973, 2025, 8, Downloaded from https://agupubs.onlinelibrary.wiley.com/doi/10.1029/2025WR040033 by Carlo Gualtieri - Uni Federico Ii Di Napoli , Wiley Online Library on [18/08/2025]. See the Terms and Conditions (https://onlinelibrary.wiley.com/terms-and-conditions) on Wiley Online Library for rules of use; OA articles are governed by the applicable Creative Commons License

19447973, 2025, 8, Downloaded from https://agupubs.onlinelibrary.wiley.com/doi/10.1029/2025WR040033 by Carlo Gualtieri - Uni Federico Ii Di Napoli , Wiley Online Library on [18/08/2025]. See the Terms and Conditions (https://onlinelibrary.wiley.com/terms-and-conditions) on Wiley Online Library for rules of use; OA articles are governed by the applicable Creative Commons License

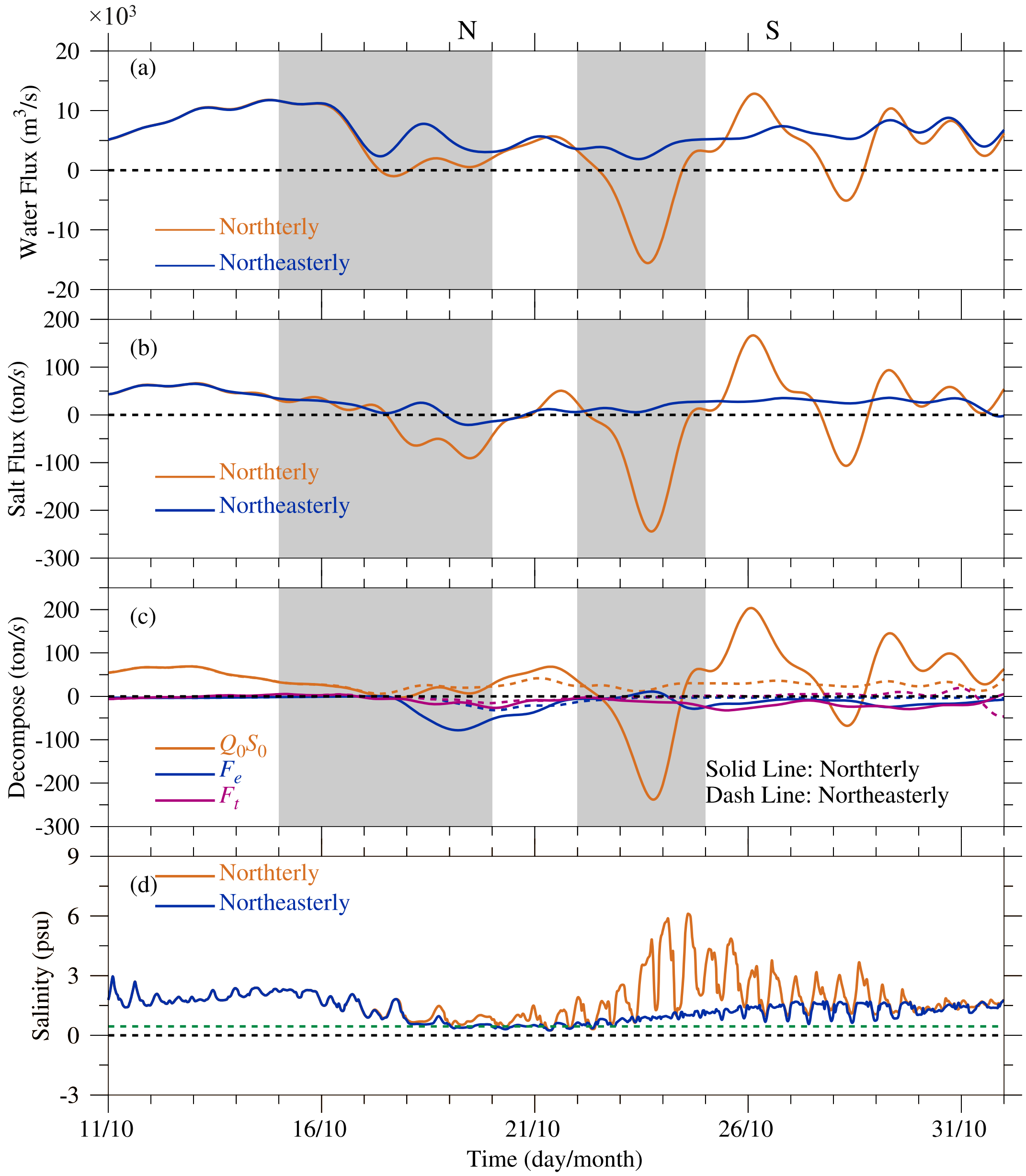

Figure 15. Daily distribution of water fluxes (a), salt fluxes (b), decomposition of total salt flux (c) and salinity (d) at the intake of the QCSR across Sec2 under different wind direction.

Both are multi-outlet estuaries influenced by seasonal runoff. However, the Mekong Estuary has a more complex distributary network, with nine main channels and shallower depths (<10 m), while the Changjiang Estuary is deeper and more channelized (Guo et al., 2021). The Mekong has a mixed semidiurnal, mesotidal regime, with spring tidal ranges of ~3.5 m near the mouth (Nowacki et al., 2015), while the Changjiang features a semi-diurnal tide dominated by the M2 constituent, with spring tidal ranges exceeding 4.5 m (H. Wu et al., 2010). Both the Changjiang and Mekong rivers show strong seasonal discharge variation, with flow ranges of 4,620–92,600 m^3/s and 2,000–40,000 m^3/s, respectively (Guo et al., 2021; Nowacki et al., 2015). This seasonal variability strongly influences estuarine mixing and salt intrusion dynamics in both systems. Both estuaries are classified as partially mixed, with stratification modulated by seasonal discharge and tidal forcing (Zeng et al., 2022). These similarities support the broader relevance of our findings, particularly regarding wind-driven salt transport and freshwater release timing, for managing saltwater intrusion in other large deltaic estuaries like the Mekong.

19447973, 2025, 8, Downloaded from https://agupubs.onlinelibrary.wiley.com/doi/10.1029/2025WR040033 by Carlo Gualtieri - Uni Federico Ii Di Napoli , Wiley Online Library on [18/08/2025]. See the Terms and Conditions (https://onlinelibrary.wiley.com/terms-and-conditions) on Wiley Online Library for rules of use; OA articles are governed by the applicable Creative Commons License

In the Changjiang River estuary, saltwater intrusion is no longer restricted to the traditional dry season. In October 2018, an atypical saltwater intrusion event was recorded during a high river discharge (>20,000 m^3/s), coinciding with the impact of Typhoon Kong-rey (Li et al., 2022). Saltwater intrusion events driven by the combined effects of extreme droughts, typhoons, and cold fronts represent a heightened threat to the utilization of freshwater resources in estuaries. Addressing saltwater intrusion under evolving environmental conditions demands more comprehensive research.

5. Conclusions

During the 2022 flood season, due to an extreme drought, the Changjiang River Estuary experienced the most severe saltwater intrusion in nearly 50 years. This study quantitatively assessed the dynamics of saltwater intrusion and the effects of the emergency freshwater release operation in the event. Since October 2, the emergency freshwater release, delivered 4.063×10^9 m^3 of freshwater. This effectively mitigated saltwater intrusion by reducing landward advective salt flux. During neap tides, the 0.45 psu isohaline moved approximately 17 km downstream, and the salinity at the QCSR decreased to around 0.45 psu on October 21, creating a 12.75-hr window for water intake. However, the available water intake time fell significantly short of expectations.

Cold fronts weakened the release effects by increasing residual water levels in the estuary and modifying estuarine circulation through wind-driven Ekman transport, facilitating landward salt flux. This process induced a horizontal circulation pattern between the NC and SC of the estuary, with enhanced salinity stratification and velocity shear in the NC. The UWNT in the NC moving landward was approximately -1 m^2/s. During the first cold front, steady shear salt flux contributed most significantly, being -70 ton/s, while advective salt flux dominated during the second cold front, reaching -239 ton/s. Without cold fronts, the potential water intake time could have increased to 36.89 hr.

For an effective freshwater release, such operation needs to be aligned in time with neap tides. Under cold front conditions, the current release strategy is optimal. Without cold fronts, advancing the current release schedule by 2 days yields the best results, with a maximum water intake period of 38.20 hr. Wind direction experiments revealed that northeasterly winds exert a minimal landward Ekman transport.

Future studies are recommended to identify the impact of freshwater release on saltwater intrusion in other tidal estuaries, such as the Mekong Estuary, to enhance freshwater resource safety in estuarine systems worldwide.

Appendix A: Model Validation

The formulas for correlation coefficient (CC), skill score (SS), and root mean square error (RMSE) are as follows:

$$CC = \frac{\sum (X_{\text{mod}} - \overline{X}_{\text{mod}})(X_{\text{obs}} - \overline{X}_{\text{obs}})}{\left[\sum (X_{\text{mod}} - \overline{X}_{\text{mod}})^2 \sum (X_{\text{obs}} - \overline{X}_{\text{obs}})^2\right]^{1/2}}; \quad \text{(A1)}$$

$$RMSE = \sqrt{\frac{\sum (X_{\text{mod}} - X_{\text{obs}})^2}{N}}; \quad \text{(A2)}$$

$$SS = 1 - \frac{\sum |X_{\text{mod}} - X_{\text{obs}}|^2}{\sum \left(|X_{\text{mod}} - \overline{X}_{\text{obs}}| + |X_{\text{obs}} - \overline{X}_{\text{obs}}|\right)^2}; \quad \text{(A3)}$$

Where X_{mod} represents the modeled data, X_{obs} represents the observed data, and $\overline{X}$ represents the average value. CC indicates the correlation between modeled and observed data. Even if there is a constant difference between the two, but their trends are consistent, a good CC evaluation result can still be obtained. Therefore, it needs to be evaluated together with RMSE to obtain an objective evaluation result. SS is used to describe the degree of deviation between modeled and observed data. When $SS \geq 0.65$, the model simulation is considered excellent; when $0.65 > SS \geq 0.5$, it is very good; when $0.5 > SS \geq 0.2$, it is good; and when $SS < 0.2$, the model simulation is deemed poor (Allen et al., 2007).

19447973, 2025, 8, Downloaded from https://agupubs.onlinelibrary.wiley.com/doi/10.1029/2025WR040033 by Carlo Gualtieri - Uni Federico Ii Di Napoli , Wiley Online Library on [18/08/2025]. See the Terms and Conditions (https://onlinelibrary.wiley.com/terms-and-conditions) on Wiley Online Library for rules of use; OA articles are governed by the applicable Creative Commons License

Acknowledgments
This work was supported by the National Key R&D Program of China (2022YFA1004404), the National Key R&D Program Young Scientist Project (2024YFC3214000), the National Natural Science Foundation of China (42276174, 42376166), the Fundamental Research Funds for Central Public Welfare Research Institutes (CKSF2025153/HL, CKSF2023189/HL). We also acknowledge the anonymous reviewers for their valuable comments and suggestions.

Data Availability Statement

The data underlying the findings of this article can be accessed at https://doi.org/10.6084/m9.figshare.28245719. The codes can be made available from the corresponding author upon reasonable request.

References

Allen, J. I., Somerfield, P. J., & Gilbert, F. J. (2007). Quantifying uncertainty in high-resolution coupled hydrodynamic-ecosystem models. *Journal of Marine Systems*, *64*(1), 3–14. https://doi.org/10.1016/j.jmarsys.2006.02.010

Aristizábal, M. F., & Chant, R. J. (2015). An observational study of salt fluxes in Delaware Bay. *Journal of Geophysical Research: Oceans*, *120*(4), 2751–2768. https://doi.org/10.1002/2014jc010680

Bellafiore, D., Ferrarin, C., Maicu, F., Manfè, G., Lorenzetti, G., Umgiesser, G., et al. (2021). Saltwater intrusion in a Mediterranean delta under a changing climate. *Journal of Geophysical Research: Oceans*, *126*(2), e2020JC016437. https://doi.org/10.1029/2020JC016437

Blumberg, A. F. (1994). *A primer for ECOM-si* (p. 66). Technical Report of HydroQual. Mahwah, New Jersey.

Casares-Salazar, R., & Mariño-Tapia, I. (2016). Influence of the remote forcing and local winds on the barotropic hydrodynamics of an elongated coastal lagoon. *Journal of Coastal Research*, *32*(1), 116–130. https://doi.org/10.2112/JCOASTRES-D-14-00146.1

Chau, M. K., Vo, Q. M., Nguyen, T. K. P., Araki, M., Perry, R. N., Tran, A. D., et al. (2021). Impacts of saltwater intrusion on soil nematodes community in alluvial and acid sulfate soils in paddy rice fields in the Vietnamese Mekong Delta. *Ecological Indicators*, *122*, 107284. https://doi.org/10.1016/j.ecolind.2020.107284

Chen, Q., Zhu, J., Lyu, H., & Chen, S. (2019). Determining critical river discharge as a means to provide water supply security to the Changjiang River Estuary, China. *Journal of Coastal Research*, *35*(5), 1087–1094. https://doi.org/10.2112/JCOASTRES-D-18-00165.1

Duran-Matute, M., Gerkema, T., & Sassi, M. G. (2016). Quantifying the residual volume transport through a multiple-inlet system in response to wind forcing: The case of the western Dutch Wadden Sea. *Journal of Geophysical Research: Oceans*, *121*(12), 8888–8903. https://doi.org/10.1002/2016JC011807

Eslami, S., Hoekstra, P., Minderhoud, P. S., Trung, N. N., Hoch, J. M., Sutanudjaja, E. H., et al. (2021). Projections of salt intrusion in a mega-delta under climatic and anthropogenic stressors. *Communications Earth & Environment*, *2*(1), 142. https://doi.org/10.1038/s43247-021-00208-5

Geyer, W. R. (1997). Influence of wind on dynamics and flushing of shallow estuaries. *Estuarine, Coastal and Shelf Science*, *44*(6), 713–722. https://doi.org/10.1006/ecss.1996.0140

Giddings, S. N., & MacCready, P. (2017). Reverse estuarine circulation due to local and remote wind forcing, enhanced by the presence of along-coast estuaries. *Journal of Geophysical Research: Oceans*, *122*(12), 10184–10205. https://doi.org/10.1002/2016JC012479

Guo, L., Zhu, C., Xie, W., Xu, F., Wu, H., Wan, Y., et al. (2021). Changjiang Delta in the Anthropocene: Multi-scale hydro-morphodynamics and management challenges. *Earth-Science Reviews*, *223*, 103850. https://doi.org/10.1016/j.earscirev.2021.103850

He, W., Zhang, J., Yu, X., Chen, S., & Luo, J. (2018). Effect of runoff variability and sea level on saltwater intrusion: A case study of Nandu River Estuary, China. *Water Resources Research*, *54*(12), 9919–9934. https://doi.org/10.1029/2018WR023285

Hoang, L. P., van Vliet, M. T. H., Kummu, M., Lauri, H., Koponen, J., Supit, I., et al. (2019). The Mekong's future flows under multiple drivers: How climate change, hydropower developments and irrigation expansions drive hydrological changes. *Science of the Total Environment*, *649*, 601–609. https://doi.org/10.1016/j.scitotenv.2018.08.160

Huang, W., & Li, C. (2017). Cold front driven flows through multiple inlets of Lake Pontchartrain Estuary. *Journal of Geophysical Research: Oceans*, *122*(11), 8627–8645. https://doi.org/10.1002/2017JC012977

Lerczak, J. A., Geyer, W. R., & Chant, R. J. (2006). Mechanisms driving the time-dependent salt flux in a partially stratified estuary. *Journal of Physical Oceanography*, *36*(12), 2296–2311. https://doi.org/10.1175/JPO2959.1

Li, L., Wang, C., Pareja-Roman, L. F., Zhu, J., Chant, R. J., & Wang, G. (2022). Effects of typhoon on saltwater intrusion in a high discharge estuary. *Journal of Geophysical Research: Oceans*, *127*(8), e2021JC018206. https://doi.org/10.1029/2021JC018206

Li, L., Zhu, J., Chant, R. J., Wang, C., & Pareja-Roman, L. F. (2020). Effect of dikes on saltwater intrusion under various wind conditions in the Changjiang Estuary. *Journal of Geophysical Research: Oceans*, *125*(7), e2019JC015685. https://doi.org/10.1029/2019JC015685

Li, L., Zhu, J., & Wu, H. (2012). Impacts of wind stress on saltwater intrusion in the Yangtze Estuary. *Science China Earth Sciences*, *55*(7), 1178–1192. https://doi.org/10.1007/s11430-011-4311-1

Li, L., Zhu, J. R., Wu, H., & Guo, Z. G. (2014). Lateral saltwater intrusion in the North Channel of the Changjiang Estuary. *Estuaries and Coasts*, *37*(1), 36–55. https://doi.org/10.1007/s12237-013-9669-1

Luo, J., Straffelini, E., Bozzolan, M., Zheng, Z., & Tarolli, P. (2024). Saltwater intrusion in the Po River Delta (Italy) during drought conditions: Analyzing its spatio-temporal evolution and potential impact on agriculture. *International Soil and Water Conservation Research*, *12*(3), 714–725. https://doi.org/10.1016/j.iswcr.2023.09.009

Lyu, H., & Zhu, J. (2018). Impact of the bottom drag coefficient on saltwater intrusion in the extremely shallow estuary. *Journal of Hydrology*, *557*, 838–850. https://doi.org/10.1016/j.jhydrol.2018.01.010

Nowacki, D. J., Ogston, A. S., Nittrouer, C. A., Fricke, A. T., & Van, P. D. T. (2015). Sediment dynamics in the lower Mekong River: Transition from tidal river to estuary. *Journal of Geophysical Research: Oceans*, *120*(9), 6363–6383. https://doi.org/10.1002/2015JC010754

Qiu, C., & Zhu, J. (2015). Assessing the influence of sea level rise on salt transport processes and estuarine circulation in the Changjiang River estuary. *Journal of Coastal Research*, *31*(3), 661–670. https://doi.org/10.2112/JCOASTRES-D-13-00138.1

Qiu, C., & Zhu, J. R. (2013). Influence of seasonal runoff regulation by the Three Gorges Reservoir on saltwater intrusion in the Changjiang River Estuary. *Continental Shelf Research*, *71*, 16–26. https://doi.org/10.1016/j.csr.2013.09.024

Van Binh, D., Kantoush, S. A., Saber, M., Mai, N. P., Maskey, S., Phong, D. T., & Sumi, T. (2020). Long-term alterations of flow regimes of the Mekong River and adaptation strategies for the Vietnamese Mekong Delta. *Journal of Hydrology: Regional Studies*, *32*, 100742. https://doi.org/10.1016/j.ejrh.2020.100742

Wu, H., & Zhu, J. (2010). Advection scheme with 3rd high-order spatial interpolation at the middle temporal level and its application to saltwater intrusion in the Changjiang Estuary. *Ocean Modelling*, *33*(1–2), 33–51. https://doi.org/10.1016/j.ocemod.2009.12.001

Wu, H., Zhu, J., Chen, B., & Chen, Y. (2006). Quantitative relationship of runoff and tide to saltwater spilling over from the North Branch in the Changjiang Estuary: A numerical study. *Estuarine, Coastal and Shelf Science*, *69*(1–2), 125–132. https://doi.org/10.1016/j.ecss.2006.04.009

Wu, H., Zhu, J., & Choi, B. H. (2010). Links between saltwater intrusion and subtidal circulation in the Changjiang Estuary: A model-guided study. *Continental Shelf Research*, *30*(17), 1891–1905. https://doi.org/10.1016/j.csr.2010.09.001

Wu, H., Zhu, J., Shen, J., & Wang, H. (2011). Tidal modulation on the Changjiang River plume in summer. *Journal of Geophysical Research*, *116*(C8), C08017. https://doi.org/10.1029/2011JC007209

Wu, T., Zhu, J., Ma, R., Qiu, W., & Yuan, R. (2023). Freshwater resources around the reclaimed new land on the Eastern Hengsha Shoal in the Changjiang estuary. *Frontiers in Marine Science*, *10*, 1302091. https://doi.org/10.3389/fmars.2023.1302091

Xue, P., Chen, C., Ding, P., Beardsley, R. C., Lin, H., Ge, J., & Kong, Y. (2009). Saltwater intrusion into the Changjiang River: A model-guided mechanism study. *Journal of Geophysical Research*, *114*(C2). https://doi.org/10.1029/2008JC004831

Yuan, R., Wu, H., Zhu, J., & Li, L. (2016). The response time of the Changjiang plume to river discharge in summer. *Journal of Marine Systems*, *154*, 82–92. https://doi.org/10.1016/j.jmarsys.2015.04.001

Zeng, X., Bracco, A., & Tagklis, F. (2022). Dynamical impact of the Mekong River plume in the South China Sea. *Journal of Geophysical Research: Oceans*, *127*(5), e2021JC017572. https://doi.org/10.1029/2021JC017572

Zhang, E., Gao, S., Savenije, H. H., Si, C., & Cao, S. (2019). Saline water intrusion in relation to strong winds during winter cold outbreaks: North Branch of the Yangtze Estuary. *Journal of Hydrology*, *574*, 1099–1109. https://doi.org/10.1016/j.jhydrol.2019.04.096

Zhu, J. R., Cheng, X., Li, L., Wu, H., Gu, J., & Lyu, H. (2020). Dynamic mechanism of an extremely severe saltwater intrusion in the Changjiang estuary in February 2014. *Hydrology and Earth System Sciences*, *24*(10), 5043–5056. https://doi.org/10.5194/hess-24-5043-2020

Zhu, J. R., Gu, Y. L., & Wu, H. (2013). Determination of the period not suitable for taking demestic water supply to the Qingcaosha Reservoir near Changjiang River estuary. *Oceanologia et Limnologia Sinica*, *44*(5), 1138–1145.

19447973, 2025, 8, Downloaded from https://agupubs.onlinelibrary.wiley.com/doi/10.1029/2025WR040033 by Carlo Gualtieri - Uni Federico Ii Di Napoli , Wiley Online Library on [18/08/2025]. See the Terms and Conditions (https://onlinelibrary.wiley.com/terms-and-conditions) on Wiley Online Library for rules of use; OA articles are governed by the applicable Creative Commons License